International Journal of Solids and Structures 46 (2009) 2577–2592

Contents lists available at ScienceDirect

International Journal of Solids and Structures

journal homepage: www.elsevier.com/locate/ijsolstr

Nonlinear micromechanical formulation of the high fidelity generalized method of cells

Rami Haj-Ali *,[1], Jacob Aboudi

School of Mechanical Engineering, Faculty of Engineering, Tel-Aviv University, Ramat-Aviv 69978, Israel

ARTICLE INFO

Article history:
Received 29 September 2008
Received in revised form 28 January 2009
Available online 20 February 2009

Keywords:
Micromechanical analysis
Computational method
Nonlinear multiphase composites
High fidelity generalized method of cells

ABSTRACT

The recent High Fidelity Generalized Method of Cells (HFGMC) micromechnical modeling framework of multiphase composites is formulated in a new form which facilitates its computational efficiency that allows an effective multiscale material–structural analysis. Towards this goal, incremental and total formulations of the governing equations are derived. A new stress update computational method is established to solve for the nonlinear material constituents along with the micromechanical equations. The method is well-suited for multiaxial finite increments of applied average stress or strain fields. Explicit matrix form of the HFGMC model is presented which allows an immediate and convenient computer implementation of the offered method. In particular, the offered derivations provide for the residual field vector (error) in its incremental and total forms along with an explicit expression for the Jacobian matrix. This enables the efficient iterative computational implementation of the HFGMC as a stand alone. Furthermore, the new formulation of the HFGMC is used to generate a nested local-global nonlinear finite element analysis of composite materials and structures. Applications are presented to demonstrate the efficiency of the proposed approach. These include the behavior of multiphase composites with nonlinearly elastic, elastoplastic and viscoplastic constituents.

1. Introduction

Classical nonlinear micromechanical models of binary composite materials have been the subject of many investigations over the last three decades. The goal of these models is predominately centered on generating the nonlinear effective response of the material and less on the local spatial variation of the deformation fields within the constituents. Reviews of this class of nonlinear and linear micromechanical methods can be found in Aboudi (1991), Christensen (1979), and Nemat-Nasser and Horii (1993), among several others. On the other hand, predicting local nonlinear mechanical behavior of periodic multiphase materials requires detailed description of the spatial deformations of the phases subject to remote loading. Therefore, refined micromechanical models are unavoidable in this case even when only considering a repeating unit-cell (RUC) due to its relative complex multiphase microstructure.

Computational nonlinear micromechanical models for multiphase RUC can be accomplished using general purpose continuum mechanics numerical methods, such as the finite-element, boundary element and finite-difference. Another analytic alternative, directly specialized for periodic multiphase composites, is the High Fidelity Generalized Method of Cells (HFGMC), expanded review of which can be found in Aboudi (2004). When using the HFGMC applied for periodic multiphase composites, the geometry of the RUC is divided into relatively small number of cells, also referred as subcells. The HFGMC employs higher order displacement expansions in the cells and employs both stress and displacement micrvariables to satisfy, on an average basis, the equilibrium equations as well as the traction and displacement continuity relations across the interfaces between the cells. In addition, the periodicity conditions are explicitly recognized in the formulation. The HFGMC can be viewed as a higher order extension of the Generalized Method of Cells (GMC) (Paley and Aboudi, 1992). It was first developed as a higher-order-theory for modeling non-periodic functionally graded composites (Aboudi et al., 1999) and for linear multi-phase periodic composite media by Aboudi et al. (2001). Arnold et al. (2004) have used this theory for the thermomechanical analysis of internally cooled structures at elevated temperatures for aerospace engine applications. The higher order theory was also used in the analysis of adhesively bonded composite joints by Bednarcyk and Yarrington (2004) and Bednarcyk et al. (2006).

One major advantage of the HFGMC model stems from its inherent ability to couple between the internal normal and shear deformations within the phases. The HFGMC has been recently applied to predict the linear, inelastic and time-dependent thermomechanical behavior of different composite material systems. Aboudi (2001) applied the HFGMC to predict the coupled electro-

* Corresponding author. Tel.: +972 3 640 8207; fax: +972 3 640 7617.
E-mail address: rami98@eng.tau.ac.il (R. Haj-Ali).
[1] On leave from Georgia Institute of Technology, Atlanta, GA 30332, USA.

0020-7683/$ - see front matter © 2009 Elsevier Ltd. All rights reserved.
doi:10.1016/j.ijsolstr.2009.02.004

magneto-thermo-elastic behavior of multiphase composites. The HFGMC was further generalized for the analysis of composites with inelastic and viscoelastic–viscoplastic phases by Aboudi et al. (2003) and Aboudi (2005), respectively. Interfacial damage in the form of fiber–matrix debonding in metal matrix composites was investigated by Bednarcyk et al. (2004) and the effect of a fiber loss was analyzed in conjunction with HFGMC by Ryvkin and Aboudi (2007). More recently Bednarcyk et al. (2008) the HFGMC was enhanced to include internal pore pressure for the analysis of foam insulation of the external tank of the space shuttle.

Efficient numerical formulation of nonlinear micromechanical analysis has received relatively less attention perhaps due to the fact that classical nonlinear micromechanical models can be integrated and solved with small incrementation schemes. These require large number of increments for an applied average stress or strain. They are effective and stable only for very small increments and predominately fixed or monotonic remote loading. Linearized incrementation methods are not capable of solving the nonlinear micromechanical equations for large or finite increments of loading, especially when large non-proportional changes occur in the local deformation fields. The latter effects are more pronounced in the case when damage, for example, is included in the formulations. Coupled micromechanical and damage formulations require proper treatment of energy dissipation and strain softening. Therefore, iterative micromechanical solution methods, with tailored stress correction schemes, are needed to capture the local and global load re-distribution that is associated with nonlinear and damage effects. Lagoudas et al. (1991) and Gavazzi and Lagoudas (1990) used the Mori–Tanaka averaging scheme based on modeling the average elastic–plastic response of the entire metallic matrix phase. They computed the Eshelby tensor using the instantaneous matrix material properties. Also, they approximated the form of the concentration tensors by making the instantaneous moduli a function of the average stresses in the matrix phase, and used the backward difference to integrate the incremental elastic–plastic equations. The method was compared to experimental and with results from the finite element hexagonal unit cell for both fibrous and particulate composites. Good agreements were obtained for particulate composites with small concentration of particles. However, in the case of fibrous composites, the Mori–Tanaka method underestimates the plastic strains under certain transverse loading paths. Doghri and Ouaar (2003) and Delannay et al. (2007) also extended the Mori–Tanaka class of nonlinear effective modeling using linearized tangential predictions and incrementations of multiphase metal matrix composites. Great care was given to the numerical formulation using consistent plasticity tangent operators and integration scheme suitable for cyclic loading and finite increments. Haj-Ali et al. (2001), Haj-Ali and Kilic (2003), Haj-Ali and Muliana (2004), Muliana and Haj-Ali (2005, 2008) and Haj-Ali (2008, 2009) developed different numerical formulations for fiber reinforced plastic (FRP) class of composites applied for the GMC and other nonlinear micromechanical models including time-dependent, nonlinear and damage effects.

The overall goal of applying the HFGMC is for refined nonlinear modeling of multiphase composites where adapted refinement of spatial variability can be performed to capture the local deformation fields. Another goal is the application of the HFGMC in a local-global multi-scale analysis of composite materials and structures. Towards these goals, the efficient nonlinear mechanical formulation and computational implementation of the HFGMC takes priority for the previously outlined arguments and in order to solve potential large-scale problems. This study presents a viable numerical integration of the HFGMC equations that allows the method to be used with arbitrary finite increments of applied mechanical loading. Incremental and total formulations of the governing equations are derived accompanied by explicit matrix form of the linearized equations. A proposed iterative computational implementation is presented and examined in its ability for rapid error reduction when finite increment of applied average strain is given. The new nonlinear formulation is suitable for implementation within displacement-based nonlinear FE structural analysis. Applications of the HFGMC with the proposed numerical formulations and implementations are presented.

The structure of this paper is outlined as follows. Section 2 presents general incremental and total nonlinear micromechanical derivations. Section 3 describes the proposed numerical algorithms and their implementations. Section 4 presents numerical applications and engineering analyses, and, finally, conclusions are given in Section 5.

2. General formulation

The HFGMC micromechanical modeling framework for doubly periodic multiphase composite media has been fully described and reviewed by Aboudi (2004). This framework is based on the homogenization technique of composites with periodic microstructure as shown in Fig. 1. The repeating unit volume of such a composite, Fig. 2, is divided into arbitrary number of rectangular cells, labeled by the indices $(\beta\gamma)$, each of which may contain a distinct nonlinear homogeneous material. The dimensions of the cell along the 2 and 3 axes are denoted by h_β and l_γ, respectively. In the present doubly periodic case of continuous fibers, a local coordinate system $(y_2^{(\beta)}, y_3^{(\gamma)})$ is introduced in each cell whose origin is located at its center, see Fig. 2.

In the framework of the HFGMC model for periodic composites, the displacement vector in the cell $(\beta\gamma)$ is given, e.g. Aboudi (2004), by the higher-order polynomial form

$$\mathbf{u}^{(\beta\gamma)} = \bar{\epsilon}\cdot\mathbf{x} + \mathbf{W}_{(00)}^{(\beta\gamma)} + y_2^{(\beta)}\mathbf{W}_{(10)}^{(\beta\gamma)} + y_3^{(\gamma)}\mathbf{W}_{(01)}^{(\beta\gamma)} + \frac{1}{2}\left(3y_2^{(\beta)2} - \frac{h_\beta^2}{4}\right)\mathbf{W}_{(20)}^{(\beta\gamma)} + \frac{1}{2}\left(3y_3^{(\gamma)2} - \frac{l_\gamma^2}{4}\right)\mathbf{W}_{(02)}^{(\beta\gamma)} \tag{1}$$

where $\bar{\epsilon}$ is the externally applied average strain. The coefficient variables vectors, $\mathbf{W}_{(mn)}^{(\beta\gamma)}$, represent the volume averaged displacement in the case of $m = n = 0$, which together with the additional higher-order terms have to be determined.

The strain vector at each cell is defined by

$$\epsilon^{(\beta\gamma)} \equiv \{\epsilon_{11}, \epsilon_{22}, \epsilon_{33}, 2\epsilon_{12}, 2\epsilon_{13}, 2\epsilon_{23}\}^{(\beta\gamma)} \tag{2}$$

After some algebraic manipulations, it is possible to represent the strain vector in the form

$$\epsilon^{(\beta\gamma)} = \bar{\epsilon} + P_{(10)}\mathbf{W}_{(10)}^{(\beta\gamma)} + P_{(01)}\mathbf{W}_{(01)}^{(\beta\gamma)} + P_{(20)}\mathbf{W}_{(20)}^{(\beta\gamma)}y_2^{(\beta)} + P_{(02)}\mathbf{W}_{(02)}^{(\beta\gamma)}y_3^{(\gamma)} \tag{3}$$

where,

$$P_{(10)} = \begin{bmatrix} 0 & 0 & 0 \\ 0 & 0 & 0 \\ 0 & 0 & 1 \\ 0 & 0 & 0 \\ 1 & 0 & 0 \\ 0 & 1 & 0 \end{bmatrix}, \qquad P_{(01)} = \begin{bmatrix} 0 & 0 & 0 \\ 0 & 1 & 0 \\ 0 & 0 & 0 \\ 1 & 0 & 0 \\ 0 & 0 & 0 \\ 0 & 0 & 1 \end{bmatrix} \tag{4}$$

and $P_{(20)} = 3P_{(10)}$, $P_{(02)} = 3P_{(01)}$.

The average strain in the cell $(\beta\gamma)$ can be identified as

$$\bar{\epsilon}^{(\beta\gamma)} = \bar{\epsilon} + P_{(10)}\mathbf{W}_{(10)}^{(\beta\gamma)} + P_{(01)}\mathbf{W}_{(01)}^{(\beta\gamma)} \tag{5}$$

The strain influence matrix $\mathbf{B}^{(\beta\gamma)}$ of the cell can be expressed in an incremental form by

$$\Delta\bar{\epsilon}^{(\beta\gamma)} \equiv \boldsymbol{B}^{(\beta\gamma)}\Delta\bar{\epsilon} = \left[\mathbf{I} + P_{(10)}\widehat{\mathbf{D}}_{(10)}^{(\beta\gamma)} + P_{(01)}\widehat{\mathbf{D}}_{(01)}^{(\beta\gamma)}\right]\Delta\bar{\epsilon} \tag{6}$$

with $\mathbf{I}$ being the identity matrix. In addition,

$$\widehat{\mathbf{D}}_{(10)}^{(\beta\gamma)}\Delta\bar{\epsilon} = \Delta\mathbf{W}_{(10)}^{(\beta\gamma)}, \qquad \widehat{\mathbf{D}}_{(01)}^{(\beta\gamma)}\Delta\bar{\epsilon} = \Delta\mathbf{W}_{(01)}^{(\beta\gamma)} \tag{7}$$

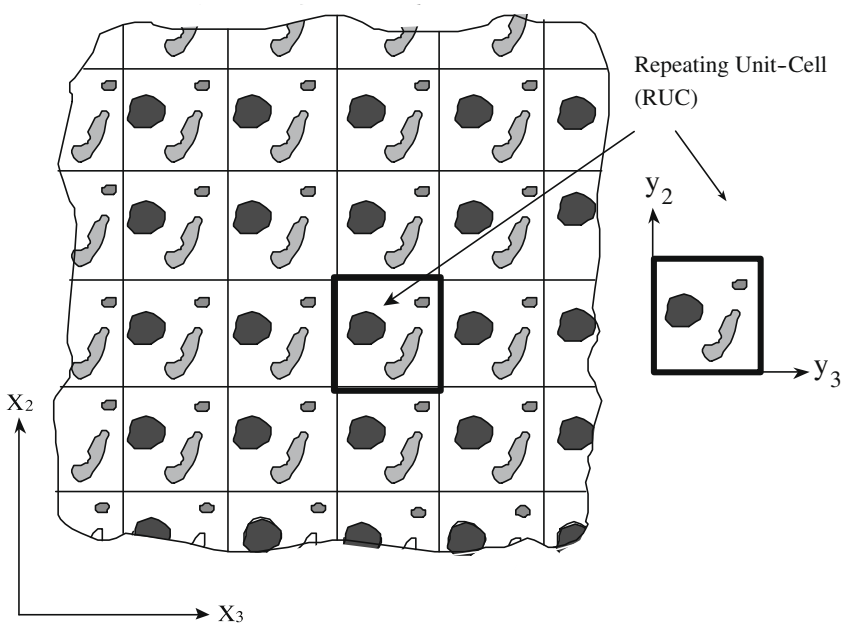

Fig. 1. Schematic illustration of a unidirectional periodic array in the global $x_2 - x_3$ plane of multiphase composite media with its repeating unit-cell (RUC), defined with respect to its $y_2 - y_3$ local coordinate system.

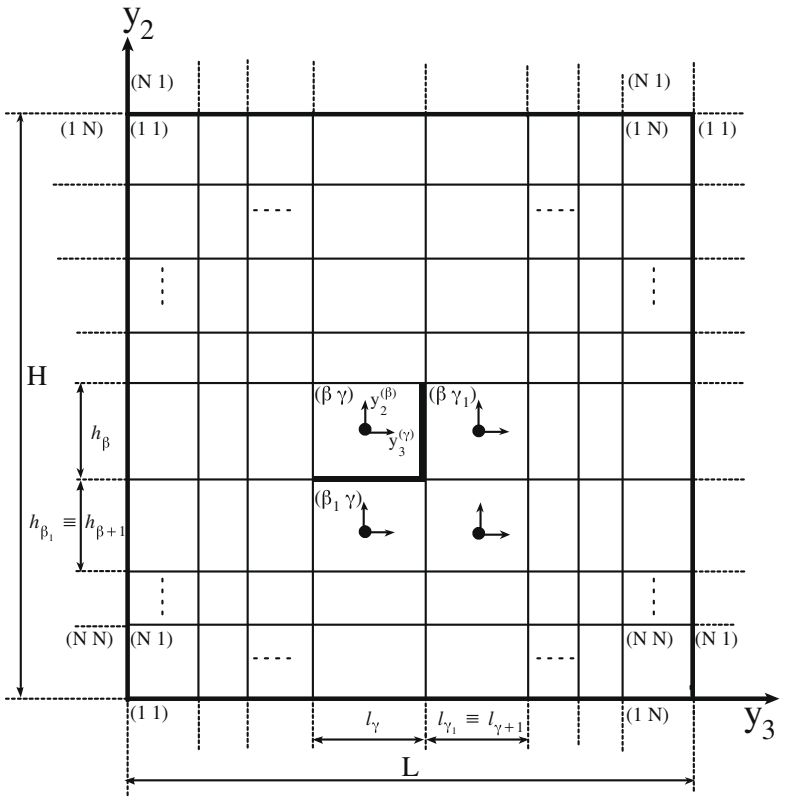

Fig. 2. General arrangement of cells and their geometry and coordinate systems for the HFGMC-RUC model. Mirrored cells-interfaces are illustrated to enforce the periodic boundary conditions.

where $\widehat{\mathbf{D}}_{(mn)}^{(\beta\gamma)}$ are determined after the solution of the entire coupled governing equations of the cells.

The resulting linear expansion of the stress vector can be expressed as

$$\boldsymbol{\sigma}^{(\beta\gamma)} = \bar{\boldsymbol{\sigma}}^{(\beta\gamma)} + \boldsymbol{\sigma}_{(10)}^{(\beta\gamma)} y_2^{(\beta)} + \boldsymbol{\sigma}_{(01)}^{(\beta\gamma)} y_3^{(\gamma)} \tag{8}$$

where $\bar{\boldsymbol{\sigma}}^{(\beta\gamma)}$ is the average stress in the cell $(\beta\gamma)$ and $\boldsymbol{\sigma}_{(mn)}^{(\beta\gamma)}$ are higher-order stresses which can be directly expressed in terms of the stress moments defined by

$$\mathbf{S}_{(mn)}^{(\beta\gamma)} = \frac{1}{h_\beta l_\gamma} \int_{-h_\beta/2}^{h_\beta/2} \int_{-l_\gamma/2}^{l_\gamma/2} \boldsymbol{\sigma}^{(\beta\gamma)} (y_2^{(\beta)})^m (y_3^{(\gamma)})^n dy_2^{(\beta)} dy_3^{(\gamma)} \tag{9}$$

These moments were previously employed in the original derivation of the HFGMC (see Aboudi, 2004). The current form of the stress vector is exactly equivalent to the original derivation:

$$\boldsymbol{\sigma}_{(10)}^{(\beta\gamma)}=\frac{12}{h_\beta^2}\mathbf{S}_{(10)}^{(\beta\gamma)},\qquad \boldsymbol{\sigma}_{(01)}^{(\beta\gamma)}=\frac{12}{l_\gamma^2}\mathbf{S}_{(01)}^{(\beta\gamma)} \tag{10}$$

The standard pointwise equilibrium equations $\nabla\cdot\boldsymbol{\sigma}=\mathbf{0}$, lead, in the framework of HFGMC theory, to the volume-average form

$$L_2\boldsymbol{\sigma}_{(10)}^{(\beta\gamma)}+L_3\boldsymbol{\sigma}_{(01)}^{(\beta\gamma)}=0 \tag{11}$$

where L_2 and L_3 are given by the Boolean matrices:

$$L_2=\begin{bmatrix}0&0&0&1&0&0\\0&1&0&0&0&0\\0&0&0&0&0&1\end{bmatrix},\qquad L_3=\begin{bmatrix}0&0&0&0&1&0\\0&0&0&0&0&1\\0&0&1&0&0&0\end{bmatrix} \tag{12}$$

For the general case of a nonlinear material filling the cell $(\beta\gamma)$, the incremental form of its constitutive relation is given by

$$\Delta\boldsymbol{\sigma}^{(\beta\gamma)}=\mathbf{C}^{(\beta\gamma)}\Delta\boldsymbol{\epsilon}^{(\beta\gamma)} \tag{13}$$

where $\mathbf{C}^{(\beta\gamma)}$ is the proper instantaneous or consistent fourth-order tangent stiffness tensor that is selected based on the considered nonlinear material behavior within the cell, such as total deformation theory, incremental plasticity, nonlinear viscoelasticity, and viscoplasticity. Standard forms of the fourth-order tangent or consistent tangent tensors for these material models can be found in Simo and Hughes (1998), Khan and Huang (1995) and ABAQUS (2007). For the particular Bodner-Partom viscoplastic theory, Bodner (2002), the time-dependent tangent tensor has been derived by Paley and Aboudi (1991) in the form

$$C_{ijkl}^{(\beta\gamma)}=\left[\lambda\delta_{ij}\delta_{kl}+\mu(\delta_{ik}\delta_{jl}+\delta_{il}\delta_{jk})-2\mu\frac{s_{rt}\dot{\epsilon}_{rt}^{P}}{s_{pq}\dot{\epsilon}_{pq}}\cdot\frac{s_{ij}s_{kl}}{s_{mn}s_{mn}}\right]^{(\beta\gamma)} \tag{14}$$

where λ and μ are the Lame' constants of the material filling the cell $(\beta\gamma)$, s_{ij} is the deviatoric part of the stress σ_{ij} in the cell, ϵ_{ij}^{P} is the corresponding plastic (inelastic) strain component and δ_{ij} is the Kronecker delta.

The incremental forms of the constitutive models for the different phases are used in the linearized formulation of the HFGMC. In addition, the corresponding total integrated constitutive forms are also employed to derive the HFGMC nonlinear equations using total microvariables and stresses in the cells.

The incremental stress is of the form

$$\Delta\boldsymbol{\sigma}^{(\beta\gamma)}=\Delta\bar{\boldsymbol{\sigma}}^{(\beta\gamma)}+\Delta\boldsymbol{\sigma}_{(10)}^{(\beta\gamma)}y_2^{(\beta)}+\Delta\boldsymbol{\sigma}_{(01)}^{(\beta\gamma)}y_3^{(\gamma)} \tag{15}$$

By substituting the incremental strain given by Eq. (3) and comparing with Eq. (15) leads to the following relations

$$\begin{aligned}\Delta\bar{\boldsymbol{\sigma}}^{(\beta\gamma)}&=\mathbf{C}^{(\beta\gamma)}\Delta\bar{\boldsymbol{\epsilon}}+\mathbf{C}^{(\beta\gamma)}P_{(10)}\Delta\mathbf{W}_{(10)}^{(\beta\gamma)}+\mathbf{C}^{(\beta\gamma)}P_{(01)}\Delta\mathbf{W}_{(01)}^{(\beta\gamma)}\\ \Delta\boldsymbol{\sigma}_{(10)}^{(\beta\gamma)}&=\mathbf{C}^{(\beta\gamma)}P_{(20)}\Delta\mathbf{W}_{(20)}^{(\beta\gamma)}\\ \Delta\boldsymbol{\sigma}_{(01)}^{(\beta\gamma)}&=\mathbf{C}^{(\beta\gamma)}P_{(02)}\Delta\mathbf{W}_{(02)}^{(\beta\gamma)}\end{aligned} \tag{16}$$

It should be noted that $\Delta\bar{\boldsymbol{\sigma}}^{(\beta\gamma)}$ is the incremental average stress in the cell. These relations are used in the equilibrium equations, Eq. (11), resulting into

$$L_2\mathbf{C}^{(\beta\gamma)}P_{(20)}\Delta\mathbf{W}_{(20)}^{(\beta\gamma)}+L_3\mathbf{C}^{(\beta\gamma)}P_{(02)}\Delta\mathbf{W}_{(02)}^{(\beta\gamma)}=0 \tag{17}$$

This equation can be equivalently expressed in the compact form

$$A_{2(20)}^{(\beta\gamma)}\Delta\mathbf{W}_{(20)}^{(\beta\gamma)}+A_{3(02)}^{(\beta\gamma)}\Delta\mathbf{W}_{(02)}^{(\beta\gamma)}=0 \tag{18}$$

where

$$A_{i(mn)}^{(\beta\gamma)}\equiv L_i\mathbf{C}^{(\beta\gamma)}P_{(mn)},\quad (mn)\neq(00) \tag{19}$$

and

$$A_{i(00)}^{(\beta\gamma)}\equiv L_i\mathbf{C}^{(\beta\gamma)} \tag{20}$$

Next, the traction and displacement continuity are imposed on an integral basis over the interfaces. Consider the two interfaces between the neighboring cells $(\beta\gamma)$ and $(\beta_1\gamma)$, and $(\beta\gamma)$ and $(\beta\gamma_1)$ where $\beta_1=\beta+1$ and $\gamma_1=\gamma+1$, the displacement continuity conditions are given by

$$\int_{-l_\gamma/2}^{l_\gamma/2}\left[\mathbf{u}^{(\beta\gamma)}\big|_{y_2^{(\beta)}=-h_\beta/2}-\mathbf{u}^{(\beta_1\gamma)}\big|_{y_2^{(\beta_1)}=h_{\beta_1}/2}\right]dy_3^{(\gamma)}=\mathbf{0} \tag{21}$$

with $\beta=1,\ldots,N_\beta-1$ and $\gamma=1,\ldots,N_\gamma$. Similarly, the displacement continuity at the interface whose normal is in the y_3-direction is

$$\int_{-h_\beta/2}^{h_\beta/2}\left[\mathbf{u}^{(\beta\gamma)}\big|_{y_3^{(\gamma)}=l_\gamma/2}-\mathbf{u}^{(\beta\gamma_1)}\big|_{y_3^{(\gamma_1)}=-l_{\gamma_1}/2}\right]dy_2^{(\beta)}=\mathbf{0} \tag{22}$$

with $\beta=1,\ldots,N_\beta$ and $\gamma=1,\ldots,N_\gamma-1$. The needed displacement periodicity conditions are

$$\int_{-l_\gamma/2}^{l_\gamma/2}\left[\mathbf{u}^{(1\gamma)}\big|_{y_2^{(1)}=h_1/2}-\mathbf{u}^{(N_\beta\gamma)}\big|_{y_2^{(N_\beta)}=-h_{N_\beta/2}}\right]dy_3^{(\gamma)}=\mathbf{0} \tag{23}$$

with $\gamma=1,\ldots,N_\gamma$.

$$\int_{-h_\beta/2}^{h_\beta/2}\left[\mathbf{u}^{(\beta1)}\big|_{y_3^{(1)}=-l_1/2}-\mathbf{u}^{(\beta N_\gamma)}\big|_{y_3^{(N_\gamma)}=l_{N_\gamma/2}}\right]dy_2^{(\beta)}=\mathbf{0} \tag{24}$$

with $\beta=1,\ldots,N_\beta$.

The two traction continuity conditions are

$$\int_{-l_\gamma/2}^{l_\gamma/2}\left[L_2\boldsymbol{\sigma}^{(\beta\gamma)}\big|_{y_2^{(\beta)}=-h_\beta/2}-L_2\boldsymbol{\sigma}^{(\beta_1\gamma)}\big|_{y_2^{(\beta_1)}=h_{\beta_1}/2}\right]dy_3^{(\gamma)}=\mathbf{0} \tag{25}$$

with $\beta=1,\ldots,N_\beta-1$ and $\gamma=1,\ldots,N_\gamma$.

$$\int_{-h_\beta/2}^{h_\beta/2}\left[L_3\boldsymbol{\sigma}^{(\beta\gamma)}\big|_{y_3^{(\gamma)}=l_\gamma/2}-L_3\boldsymbol{\sigma}^{(\beta\gamma_1)}\big|_{y_3^{(\gamma_1)}=-l_{\gamma_1}/2}\right]dy_2^{(\beta)}=\mathbf{0} \tag{26}$$

with $\beta=1,\ldots,N_\beta$ and $\gamma=1,\ldots,N_\gamma-1$. The needed traction periodicity conditions are

$$\int_{-l_\gamma/2}^{l_\gamma/2}\left[L_2\boldsymbol{\sigma}^{(1\gamma)}\big|_{y_2^{(1)}=h_1/2}-L_2\boldsymbol{\sigma}^{(N_\beta\gamma)}\big|_{y_2^{(N_\beta)}=-h_{N_\beta/2}}\right]dy_3^{(\gamma)}=\mathbf{0} \tag{27}$$

with $\gamma=1,\ldots,N_\gamma$.

$$\int_{-h_\beta/2}^{h_\beta/2}\left[L_3\boldsymbol{\sigma}^{(\beta1)}\big|_{y_3^{(1)}=-l_1/2}-L_3\boldsymbol{\sigma}^{(\beta N_\gamma)}\big|_{y_3^{(N_\gamma)}=l_{N_\gamma/2}}\right]dy_2^{(\beta)}=\mathbf{0} \tag{28}$$

with $\beta=1,\ldots,N_\beta$. It should be emphasized that the periodicity relations, Eqs. (23),(24) and (27),(28), are satisfied by mirroring and extending the cells near the periodic interfaces as shown in Fig. 2. Therefore Eqs. (21),(22) and (25),(26) are equivalent to the periodic relations by using the proposed mirroring technique. For example, the continuity equations can be applied to satisfy the periodicity conditions by simply performing the shifting operation: $(\beta=N_\beta+1,\gamma)\Rightarrow(1,\gamma)$. Thus Eqs. (21),(22) and (25),(26) can be applied using the outlined mirroring procedure to enforce the periodicity conditions as well.

The four displacement and traction continuity equations, Eqs. (21),(22) and (25),(26), can be expressed in the incremental form:

$$\begin{aligned}&\left[\Delta\mathbf{W}_{(00)}^{(\beta\gamma)}-\frac{h_\beta}{2}\Delta\mathbf{W}_{(10)}^{(\beta\gamma)}+\frac{h_\beta^2}{4}\Delta\mathbf{W}_{(20)}^{(\beta\gamma)}\right]\\ &-\left[\Delta\mathbf{W}_{(00)}^{(\beta_1\gamma)}+\frac{h_{\beta_1}}{2}\Delta\mathbf{W}_{(10)}^{(\beta_1\gamma)}+\frac{h_{\beta_1}^2}{4}\Delta\mathbf{W}_{(20)}^{(\beta_1\gamma)}\right]=\mathbf{0}\end{aligned} \tag{29}$$

$$\left[\Delta\mathbf{W}^{(\beta\gamma)}_{(00)}+\frac{l_\gamma}{2}\Delta\mathbf{W}^{(\beta\gamma)}_{(01)}+\frac{l_\gamma^2}{4}\Delta\mathbf{W}^{(\beta\gamma)}_{(02)}\right] - \left[\Delta\mathbf{W}^{(\beta\gamma_1)}_{(00)}-\frac{l_{\gamma_1}}{2}\Delta\mathbf{W}^{(\beta\gamma_1)}_{(01)}+\frac{l_{\gamma_1}^2}{4}\Delta\mathbf{W}^{(\beta\gamma_1)}_{(02)}\right]=\mathbf{0} \tag{30}$$

$$\left[\mathbf{A}^{(\beta\gamma)}_{2(10)}\Delta\mathbf{W}^{(\beta\gamma)}_{(10)}+\mathbf{A}^{(\beta\gamma)}_{2(01)}\Delta\mathbf{W}^{(\beta\gamma)}_{(01)}-\frac{h_\beta}{2}\mathbf{A}^{(\beta\gamma)}_{2(20)}\Delta\mathbf{W}^{(\beta\gamma)}_{(20)}\right] - \left[\mathbf{A}^{(\beta_1\gamma)}_{2(10)}\Delta\mathbf{W}^{(\beta_1\gamma)}_{(10)}+\mathbf{A}^{(\beta_1\gamma)}_{2(01)}\Delta\mathbf{W}^{(\beta_1\gamma)}_{(01)}+\frac{h_{\beta_1}}{2}\mathbf{A}^{(\beta_1\gamma)}_{2(20)}\Delta\mathbf{W}^{(\beta_1\gamma)}_{(20)}\right] = \left[\mathbf{A}^{(\beta_1\gamma)}_{2(00)}-\mathbf{A}^{(\beta\gamma)}_{2(00)}\right]\Delta\bar{\boldsymbol{\epsilon}} \tag{31}$$

$$\left[\mathbf{A}^{(\beta\gamma)}_{3(10)}\Delta\mathbf{W}^{(\beta\gamma)}_{(10)}+\mathbf{A}^{(\beta\gamma)}_{3(01)}\Delta\mathbf{W}^{(\beta\gamma)}_{(01)}+\frac{l_\gamma}{2}\mathbf{A}^{(\beta\gamma)}_{3(02)}\Delta\mathbf{W}^{(\beta\gamma)}_{(02)}\right] - \left[\mathbf{A}^{(\beta\gamma_1)}_{3(10)}\Delta\mathbf{W}^{(\beta\gamma_1)}_{(10)}+\mathbf{A}^{(\beta\gamma_1)}_{3(01)}\Delta\mathbf{W}^{(\beta\gamma_1)}_{(01)}-\frac{l_{\gamma_1}}{2}\mathbf{A}^{(\beta\gamma_1)}_{3(02)}\Delta\mathbf{W}^{(\beta\gamma_1)}_{(02)}\right] = \left[\mathbf{A}^{(\beta\gamma_1)}_{3(00)}-\mathbf{A}^{(\beta\gamma)}_{3(00)}\right]\Delta\bar{\boldsymbol{\epsilon}} \tag{32}$$

Let us define the vector of incremental variables of each $(\beta\gamma)$ cell as

$$\Delta\mathbf{X}^{(\beta\gamma)}\equiv\left\{\Delta\mathbf{W}_{(10)},\Delta\mathbf{W}_{(01)},\Delta\mathbf{W}_{(00)},\Delta\mathbf{W}_{(20)},\Delta\mathbf{W}_{(02)}\right\}^{(\beta\gamma)} \tag{33}$$

Fig. 3 illustrates the common interfaces between a cell $(\beta\gamma)$ and its neighboring cells. As previously shown, it is sufficient to consider the continuity conditions at the two interfaces $y_2=h_\beta/2$ and $y_3=l_\gamma/2$ (illustrated by bold lines in Fig. 3).

The increment of the residual vector $\boldsymbol{R}^{(\beta\gamma)}$ for the governing equations is arranged in the order of traction continuity, Eqs. (31),(32), the internal equilibrium equations for the cell, Eq. (18), followed by the displacement continuity, Eqs. (29),(30), written for the above two interfaces:

$$\begin{aligned}\Delta\boldsymbol{R}^{(\beta\gamma)}&\equiv\left\{\Delta\mathbf{R}_\sigma,\ \Delta\mathbf{R}_E,\ \Delta\mathbf{R}_u\right\}^{(\beta\gamma)}\\&=\mathbf{T}_1^{(\beta\gamma)}\Delta\mathbf{X}^{(\beta\gamma)}+\mathbf{T}_2^{(\beta_1\gamma)}\Delta\mathbf{X}^{(\beta_1\gamma)}+\mathbf{T}_3^{(\beta\gamma_1)}\Delta\mathbf{X}^{(\beta\gamma_1)}\\&\quad-\mathbf{D}_1^{(\beta\gamma)}\Delta\bar{\boldsymbol{\epsilon}}-\mathbf{D}_2^{(\beta_1\gamma)}\Delta\bar{\boldsymbol{\epsilon}}-\mathbf{D}_3^{(\beta\gamma_1)}\Delta\bar{\boldsymbol{\epsilon}}\end{aligned} \tag{34}$$

The matrix $\mathbf{T}_1^{(\beta\gamma)}$ operates on the incremental microvariable vector $\Delta\mathbf{X}^{(\beta\gamma)}$ and provides the incremental traction and displacement at the two interfaces within the cell $(\beta\gamma)$. Its structure is given by

$$\mathbf{T}_1^{(\beta\gamma)}=\begin{bmatrix}\mathbf{A}_{2(10)}&\mathbf{A}_{2(01)}&\mathbf{0}&-\frac{h_\beta}{2}\mathbf{A}_{2(20)}&\mathbf{0}\\\mathbf{A}_{3(10)}&\mathbf{A}_{3(01)}&\mathbf{0}&\mathbf{0}&\frac{l_\gamma}{2}\mathbf{A}_{3(02)}\\\mathbf{0}&\mathbf{0}&\mathbf{0}&\mathbf{A}_{2(20)}&\mathbf{A}_{3(02)}\\-\frac{h_\beta}{2}\mathbf{I}&\mathbf{0}&\mathbf{I}&\frac{h_\beta^2}{4}\mathbf{I}&\mathbf{0}\\\mathbf{0}&\frac{l_\gamma}{2}\mathbf{I}&\mathbf{I}&\mathbf{0}&\frac{l_\gamma^2}{4}\mathbf{I}\end{bmatrix}^{(\beta\gamma)} \tag{35}$$

Similarly, the matrices $\mathbf{T}_2^{(\beta_1\gamma)}$ and $\mathbf{T}_3^{(\beta\gamma_1)}$ operate on the incremental microvariable vectors, $\Delta\mathbf{X}^{(\beta_1\gamma)}$ and $\Delta\mathbf{X}^{(\beta\gamma_1)}$ of the adjacent cells, respectively. They provide the incremental traction and displacement on the other side of the two interfaces. For example, the matrix $\mathbf{T}_3^{(\beta\gamma_1)}$ provides the incremental displacement and stress within the cell $(\beta\gamma_1)$ needed to complete the continuity conditions at the common interface of the adjacent cell $(\beta\gamma)$. These two matrices are of the form

$$\mathbf{T}_2^{(\beta_1\gamma)}=\begin{bmatrix}-\mathbf{A}_{2(10)}&-\mathbf{A}_{2(01)}&\mathbf{0}&-\frac{h_\beta}{2}\mathbf{A}_{2(20)}&\mathbf{0}\\\mathbf{0}&\mathbf{0}&\mathbf{0}&\mathbf{0}&\mathbf{0}\\\mathbf{0}&\mathbf{0}&\mathbf{0}&\mathbf{0}&\mathbf{0}\\-\frac{h_\beta}{2}\mathbf{I}&\mathbf{0}&-\mathbf{I}&-\frac{h_\beta^2}{4}\mathbf{I}&\mathbf{0}\\\mathbf{0}&\mathbf{0}&\mathbf{0}&\mathbf{0}&\mathbf{0}\end{bmatrix}^{(\beta_1\gamma)} \tag{36}$$

$$\mathbf{T}_3^{(\beta\gamma_1)}=\begin{bmatrix}\mathbf{0}&\mathbf{0}&\mathbf{0}&\mathbf{0}&\mathbf{0}\\-\mathbf{A}_{3(10)}&-\mathbf{A}_{3(01)}&\mathbf{0}&\mathbf{0}&\frac{l_{\gamma_1}}{2}\mathbf{A}_{3(02)}\\\mathbf{0}&\mathbf{0}&\mathbf{0}&\mathbf{0}&\mathbf{0}\\\mathbf{0}&\mathbf{0}&\mathbf{0}&\mathbf{0}&\mathbf{0}\\\mathbf{0}&\frac{l_{\gamma_1}}{2}\mathbf{I}&-\mathbf{I}&\mathbf{0}&-\frac{l_\gamma^2}{4}\mathbf{I}\end{bmatrix}^{(\beta\gamma_1)} \tag{37}$$

The $\mathbf{D}_i$ matrices can be viewed as the contribution to the local stresses at the considered two interfaces of the corresponding cells from the externally applied global strain field. Their structure is given by

$$\mathbf{D}_1^{(\beta\gamma)}=\begin{bmatrix}-\mathbf{A}_{2(00)}\\-\mathbf{A}_{3(00)}\\\mathbf{0}\\\mathbf{0}\\\mathbf{0}\\\mathbf{0}\end{bmatrix}^{(\beta\gamma)}\quad\mathbf{D}_2^{(\beta_1\gamma)}=\begin{bmatrix}\mathbf{A}_{2(00)}\\\mathbf{0}\\\mathbf{0}\\\mathbf{0}\\\mathbf{0}\\\mathbf{0}\end{bmatrix}^{(\beta_1\gamma)}\quad\mathbf{D}_3^{(\beta\gamma_1)}=\begin{bmatrix}\mathbf{0}\\\mathbf{A}_{3(00)}\\\mathbf{0}\\\mathbf{0}\\\mathbf{0}\\\mathbf{0}\end{bmatrix}^{(\beta\gamma_1)} \tag{38}$$

It is interesting to note that the displacement continuity and equilibrium equations expressed in terms of the incremental microvariables result in a set of homogeneous algebraic equations. This fact is useful for condensation purposes of the overall system of equations as will be shown later.

The final system of the tangential governing equations is obtained by assembling the contributions from all the cells by utilizing the expressions given by Eq. (34). Fig. 4 illustrates the form of the global tangential system of equations highlighting the contribution of a general cell $(\beta\gamma)$. The expanded form of the vector of variables is

$$\Delta\mathbf{X}=\left\{\Delta\mathbf{X}^{(11)},\Delta\mathbf{X}^{(12)},\ldots,\Delta\mathbf{X}^{(N_\beta N_\gamma)}\right\} \tag{39}$$

Alternatively, it is possible to perform the assembly on a cell-by-cell basis where in such a case all indicted matrices in this figure will be solely computed from the cell stiffness and assembled on a column basis.

It is possible to dramatically reduce the computational effort by employing a condensation procedure. To this end, the previously identified homogeneous and non-homogeneous equations at the cell level can be grouped into two parts. The re-partitioned system has the form

$$\begin{bmatrix}\mathbf{A}_{\sigma\sigma}&\mathbf{A}_{\sigma u}\\\mathbf{A}_{u\sigma}&\mathbf{A}_{uu}\end{bmatrix}\begin{Bmatrix}\Delta\mathbf{X}_\sigma\\\Delta\mathbf{X}_u\end{Bmatrix}=\begin{bmatrix}\mathbf{D}\\\mathbf{0}\end{bmatrix}\{\Delta\bar{\boldsymbol{\epsilon}}\} \tag{40}$$

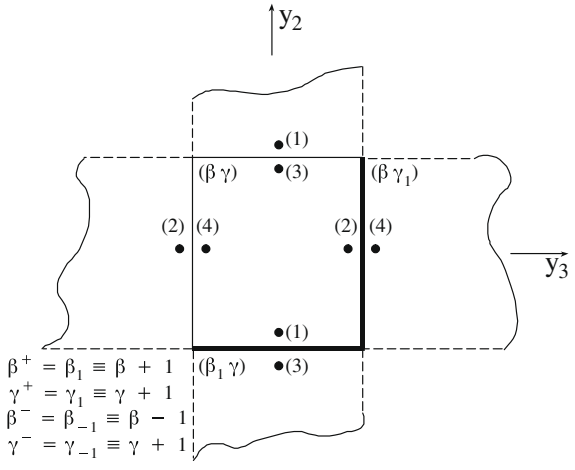

Fig. 3. One-cell configuration with its neighboring cells showing its two primary "feed-forward" interfaces along with the location for the stress integration points.

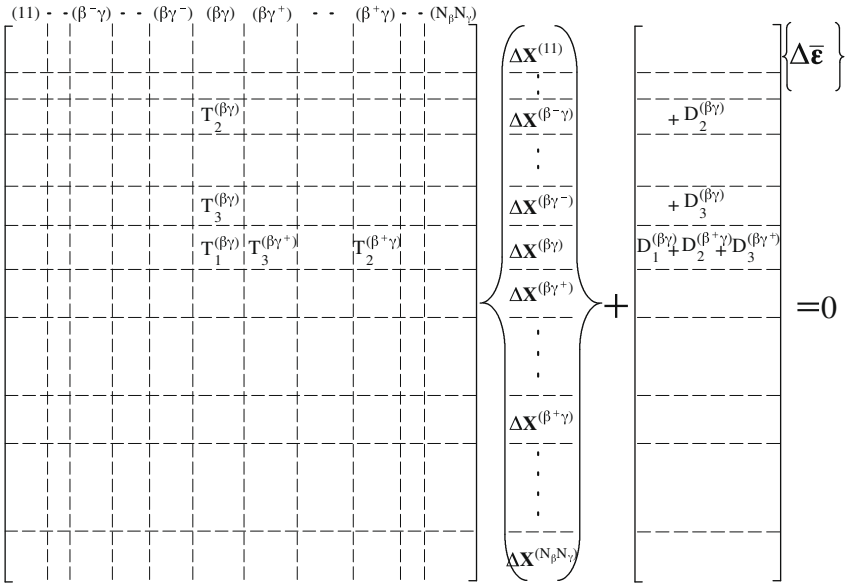

Fig. 4. Overall tangential system of equations for the HFGMC-RUC model indicating the contribution of cell $(\beta\gamma)$ to the system and showing a row of complete equations for this cell.

The terms $\mathbf{A}_{\sigma\sigma}$ and $\mathbf{A}_{uu}$ in Eq. (40) involve the traction continuity (non-homogeneous equations) on the one hand, and the equilibrium and displacement continuity (homogeneous equations) on the other hand. The off diagonal terms $\mathbf{A}_{\sigma u}$ and $\mathbf{A}_{u\sigma}$ involve the mixed terms that emerge from re-partitioning the system of equations. The two parts of the vector of variables, $\Delta\mathbf{X}_\sigma$ and $\Delta\mathbf{X}_u$, have similar definitions. The solution can be represented symbolically as:

$$\Delta\mathbf{X} = \mathbf{A}^{-1}\mathbf{D}\Delta\bar{\epsilon} \equiv \widehat{\mathbf{D}}\Delta\bar{\epsilon} \tag{41}$$

where the square matrix $\mathbf{A}$ that appears on the left-hand-side of Eq. (40) has the dimension $15N_\beta N_\gamma \times 15N_\beta N_\gamma$ in a non-condensed form. However, by performing the condensation procedure the dimension of the condensed system reduces to $6N_\beta N_\gamma \times 6N_\beta N_\gamma$.

The overall (global) tangential stiffness matrix defined from the effective incremental stress–strain relation, $\Delta\bar{\sigma} = \mathbf{C}^*\Delta\bar{\epsilon}$, of the composite can be obtained by determining the influence matrices $\mathbf{B}^{(\beta\gamma)}$ defined by the incremental form of Eqs. (5)–(7). The needed matrices $\widehat{\mathbf{D}}^{(\beta\gamma)}_{(10)}$ and $\widehat{\mathbf{D}}^{(\beta\gamma)}_{(01)}$ can be identified from $\widehat{\mathbf{D}}$ in Eq. (41) which can be partitioned as follows

$$\widehat{\mathbf{D}}^{(\beta\gamma)} = \begin{bmatrix} \widehat{\mathbf{D}}_{(10)} \\ \widehat{\mathbf{D}}_{(01)} \\ \widehat{\mathbf{D}}_{(00)} \\ \widehat{\mathbf{D}}_{(20)} \\ \widehat{\mathbf{D}}_{(02)} \end{bmatrix}^{(\beta\gamma)}, \tag{42}$$

Consequently, the effective tangential stiffness of the composite can be readily evaluated as follows (Haj-Ali, 2008; Aboudi, 2008)

$$\mathbf{C}^* = \frac{1}{HL}\sum_{\beta=1}^{N_\beta}\sum_{\gamma=1}^{N_\gamma} h_\beta l_\gamma \mathbf{C}^{(\beta\gamma)}\mathbf{B}^{(\beta\gamma)} \equiv \sum_{\beta=1}^{N_\beta}\sum_{\gamma=1}^{N_\gamma} h_\beta l_\gamma \mathbf{B}^{T(\beta\gamma)}\mathbf{C}^{T(\beta\gamma)} \tag{43}$$

which shows the symmetry of the effective tangential stiffness of the composite.

Next, we derive the residual vector of the governing equation for a characteristic cell $(\beta\gamma)$ that is needed in order to obtain the error of the nonlinear system during the iterative solution. The total (rather than incremental) interfacial displacements and stresses are determined from the total strains derived from the trial microvariables. These field variables are evaluated at both sides of the neighboring cells as illustrated in Fig. 3. The locations of the integration stress points are indicated by the solid circles. It should be noted that the displacement residuals are explicitly zero since they do not involve stiffness variables. The residual vector of cell $(\beta\gamma)$ is given by:

$$\mathbf{R}^{(\beta\gamma)} = \begin{bmatrix} \int[L_2\boldsymbol{\sigma}^{(\beta\gamma)} - L_2\boldsymbol{\sigma}^{(\beta_1\gamma)}]dy_3^{(\gamma)} \\ \int[L_3\boldsymbol{\sigma}^{(\beta\gamma)} - L_3\boldsymbol{\sigma}^{(\beta\gamma_1)}]dy_2^{(\beta)} \\ L_2\boldsymbol{\sigma}^{(\beta\gamma)}_{(10)} - L_3\boldsymbol{\sigma}^{(\beta\gamma)}_{(01)} \\ 0 \\ 0 \end{bmatrix} \rightarrow \begin{bmatrix} L_2\boldsymbol{\sigma}^{(\beta\gamma)_1} - L_2\boldsymbol{\sigma}^{(\beta_1\gamma)_3} \\ L_3\boldsymbol{\sigma}^{(\beta\gamma)_2} - L_3\boldsymbol{\sigma}^{(\beta\gamma_1)_4} \\ L_2\boldsymbol{\sigma}^{(\beta\gamma)}_{(10)} - L_3\boldsymbol{\sigma}^{(\beta\gamma)}_{(01)} \\ 0 \\ 0 \end{bmatrix} \tag{44}$$

where the first two components define the traction continuities in a total form, whereas the third term stands for the total form of the equilibrium equations in the cell. The transition from the mathematical definition of the residual vector to its numerical form is expressed by the two parts of Eq. (44). The equilibrium equations involve higher-order stresses that are obtained from the total stress values evaluated at the stress integration points:

$$\boldsymbol{\sigma}^{(\beta\gamma)}_{(10)} = \frac{1}{h_\beta}\left(\boldsymbol{\sigma}^{(\beta\gamma)_3} - \boldsymbol{\sigma}^{(\beta\gamma)_2}\right); \qquad \boldsymbol{\sigma}^{(\beta\gamma)}_{(01)} = \frac{1}{l_\gamma}\left(\boldsymbol{\sigma}^{(\beta\gamma)_2} - \boldsymbol{\sigma}^{(\beta\gamma)_4}\right) \tag{45}$$

The cell's residual vector $\mathbf{R}^{(\beta\gamma)}$ is used in the process of assembling the overall residual vector of the HFGMC model $\mathbf{R}_{HFGMC}$ given by

$$\mathbf{R}_{HFGMC} = \left\{\mathbf{R}^{(11)}, .., \mathbf{R}^{(\beta\gamma)}, .., \mathbf{R}^{(N_\beta N_\gamma)}\right\} \tag{46}$$

This residual vector should be equal to zero in order to solve for the nonlinear HFGMC equations. This is numerically achieved by requiring that its norm should be sufficiently small. In the case where a mixed stress and strain combination is applied (e.g., a uniaxial transverse loading defined by: $\bar{\epsilon}_{22} \neq 0$ and $\bar{\sigma}_{ij} = 0$ for all other components), an additional global residual vector, $\mathbf{R}_G$, must be introduced, (for the above uniaxial transverse loading, $\mathbf{R}_G = \{\bar{\sigma}_{11}, \bar{\sigma}_{33}, \bar{\sigma}_{23}, \bar{\sigma}_{13}, \bar{\sigma}_{12}\}$), The condition that $\mathbf{R}_G = \mathbf{0}$ should be satisfied together with $\mathbf{R}_{HFGMC} = \mathbf{0}$.

3. Numerical Implementation of HFGMC

Recent advances in computer technology have made it possible and practical for carrying out refined analysis of composite

1. Input variables: $\Delta\bar{\varepsilon}^{t}_{ij}$; Δt

Recall prior converged solution state:

$$\bar{\varepsilon}^{t-\Delta t}\ ;\ \bar{\sigma}^{t-\Delta t}\ ;\ \text{Hist}^{t-\Delta t} : \{W,\ \sigma,\ \text{Hist\_m}\}^{(\beta\gamma),t-\Delta t}$$

2. Initialize linearized state and perform trial tangential update

$$W^{(\beta\gamma),t-\Delta t} \rightarrow \varepsilon^{(\beta\gamma),t-\Delta t}\ ;\quad \text{Hist}^{(\beta\gamma),t-\Delta t} \rightarrow C^{(\beta\gamma),t-\Delta t} \qquad \text{Eq. (5)}$$

Assemble overall system and solve for: $A\,\Delta X \equiv J^{i=0}\,\Delta X = D\,\Delta\bar{\varepsilon}$ Eq. (40)

$$\Delta X \rightarrow \Delta W^{(\beta\gamma);i=0}$$

3. Iterate for i=1, 2, 3....

3.1 Evaluate trial microvariables $W^{(\beta\gamma),t-\Delta t} + \Delta W^{(\beta\gamma),i-1} \rightarrow W^{(\beta\gamma),i}$

3.2 Evaluate trial incremental and total strains at all cells:

$$W^{(\beta\gamma),i} \rightarrow \varepsilon^{(\beta\gamma),i} \qquad \text{Eq.(5)}$$

3.3 Perform total or incremental constitutive stress update at all integration points within all cells to get:

$$\sigma^{(\beta\gamma),t}\ ;\ \text{Hist}^{(\beta\gamma),t}\ ;\ C^{(\beta\gamma),t}$$

3.4 Assemble residual error vector: $R^{(\beta\gamma),t} \rightarrow R^{t}_{HFGMC}$ Eqs.(44,46)

IF $\| R^{t}_{HFGMC} \| \le \text{Tol}$ THEN GOTO 4 and EXIT

ELSE

3.5 Compute the correction for the microvariables:

$$\Delta X^{i} \equiv X^{i} - X^{i-1} = -\left[\frac{\partial R^{t}_{HFGMC}}{\partial \Delta W^{t}}\right]^{-1}_{i-1} R^{t}_{HFGMC} = \left[J^{i-1,t}\right]^{-1} R^{t}_{HFGMC} \qquad \text{Eq.(41)}$$

$$\Delta X^{i} \rightarrow \Delta W^{(\beta\gamma),i}$$

REJECT: $\sigma^{(\beta\gamma),t}\ ;\ \text{Hist}^{(\beta\gamma),t}\ ;\ C^{(\beta\gamma),t}$

Assemble $J^{i} \equiv A^{i}$ and GOTO 3

ENDIF

4. Update local microvariables, stresses, overall effective tangent stiffness:

$$W^{(\beta\gamma),i} \rightarrow W^{(\beta\gamma),t}\ ;\ \text{Hist}^{t} : \{W,\ \sigma,\ \text{Hist\_m}\}^{(\beta\gamma),t,i}\ ;\ C^{*}\ ;\ \bar{\sigma}$$

EXIT

Fig. 5. Iterative solution algorithm using the new nonlinear HFGMC formulation: incremental and total formulations with stress update-correction.

structures including nonlinear effects. The use of nonlinear stress–strain relations, such as those provided by plasticity and other inelastic models, is now considered a standard engineering practice. However, nonlinear modeling approaches that couple three-dimensional micromechanical and structural analysis are not widespread for laminated composite structures. Such coupled nonlinear 3D micromechanical-structural analysis may be needed in order to produce reliable structural designs. Realistic nonlinear and 3D constitutive models are needed to depict accurately the structural response in the presence of edge effects and discontinuities. These discontinuities, such as crack tips, holes, and cutouts, usually have a significant impact on the response of the structure, because damage and failure will typically initiate at and propagate from these locations.

In the present section, the previous analytical derivation of the HFGMC model is numerically implemented for the nonlinear stress analysis of multiphase materials and composite structures. To this end, the numerical algorithm of this implementation proceeds as follows. Given a finite-size of an average strain increment and the history of deformations in the cells, the strain interaction matrices, $\mathbf{B}^{(\beta\gamma)}$, are first evaluated after establishing the solution given by Eq. (41). This linearized solution results from the implementation of the tangential equations, namely, the equilibrium equations of the cells, the incremental traction and displacement interfacial continuities along with periodic conditions, all expressed with the increments of the microvariables. This linearized stress analysis will be referred to as the trial state. However, if this trial solution is accepted, two types of errors will result and accumulate. The first error occurs in the predicted strain increments $\Delta\bar{\epsilon}^{(\beta\gamma)}$ because the strain interaction matrices are derived using the tangent stiffness matrices $\mathbf{C}^{(\beta\gamma)}$ of Eq. (13) of

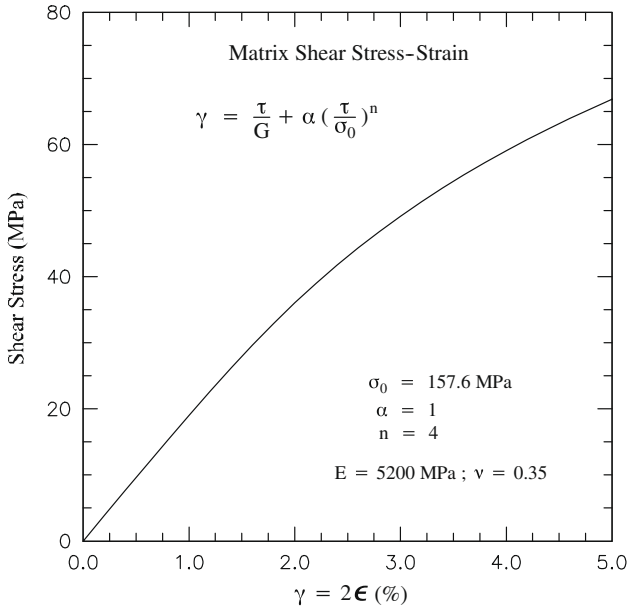

Fig. 6. Matrix shear stress–strain curve using the Ramberg-Osgood nonlinear equation form.

the cells at the beginning of the increment. The second error occurs as a result of using the tangent stiffness matrices to compute the spatial stress increments $\bar{\sigma}^{(\beta\gamma)}$, Eq. (15), in the cells for this trial state. It is important to mention that while the above two errors occur, the incremental micromechnical equations (equilibrium, displacement and traction continuity, and periodicity constraints) are satisfied by the trial state. However, the latter micromechanical constraints are satisfied with increasingly inaccurate deformation (total stress and strain) states in the cells. Therefore, a correction procedure must be used in order to accurately integrate the nonlinear constitutive material behavior and simultaneously satisfy the micromechanical equations.

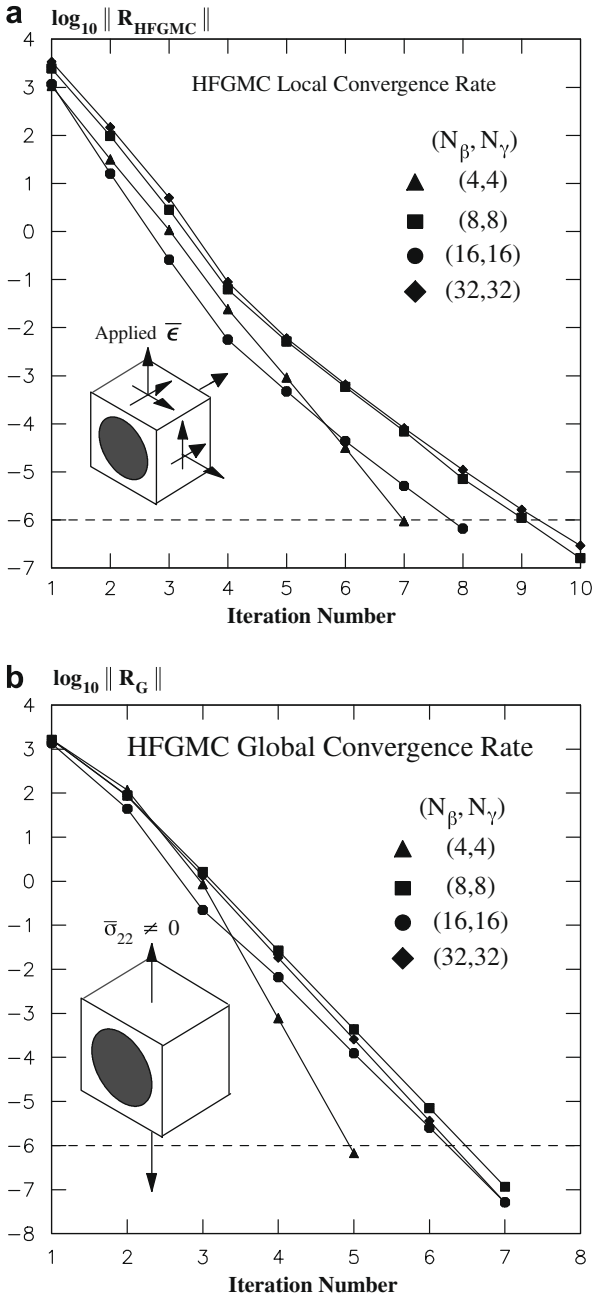

Fig. 7. Error reduction and convergence of the HFGMC for nonlinear glass/epoxy composite with applied transverse loading. (a) Local error convergence measure for $\mathbf{R}_{HFGMC}$ when the composite is subjected to a general multi-axial strain increment. (b) Global $\mathbf{R}_G$ convergence measure of the effort to minimize the effective stress residual.

The derived incremental HFGMC micromechanical relations are exact only in the case of linear stress–strain relations in the fiber and matrix cells. Due to a nonlinear response in one or more of the cells, the tangential relations will, as mentioned above, violate the constitutive equations. Hence, an iterative correction scheme is needed in order to satisfy both the micromechanical constraints and the constitutive equations. The tasks for the developed micromechanical algorithm can be stated as follows. Given the history of field variables in the cells from previous converged solution and a constant average strain rate for the RUC within the current time increment, one needs to update the effective stress, effective stiffness, and the history variables at the end of the increment. Fig. 5 illustrates the proposed iterative correction algorithm developed for the HFGMC modeling framework. The first step in this figure describes the established converged solution from the previous increment. In Step-2, the trial tangential state is solved and the incremental displacement microvariables are determined. Next, the iterative procedure starts by evaluating the total form of the trial microvriables, see step 3.1. The strain increments are subsequently evaluated at the integration points in each of the cells. In turn, the total stresses are evaluated as illustrated in steps 3.2 and 3.3 in Fig. 5 by solving the appropriate nonlinear constitutive equation of the material within the cell. The residual error vector $\mathbf{R}_{HFGMC}$ is formed and its norm can be equated to a small given tolerance, see steps 3.4 and 3.5. In the case of no convergence, improved trial increments of the microvariables are achieved by using a Newton–Raphson type nonlinear solution method as shown in step 3.5 of the iterative algorithm in Fig. 5. The stress and strain states that satisfy the constitutive relations but not

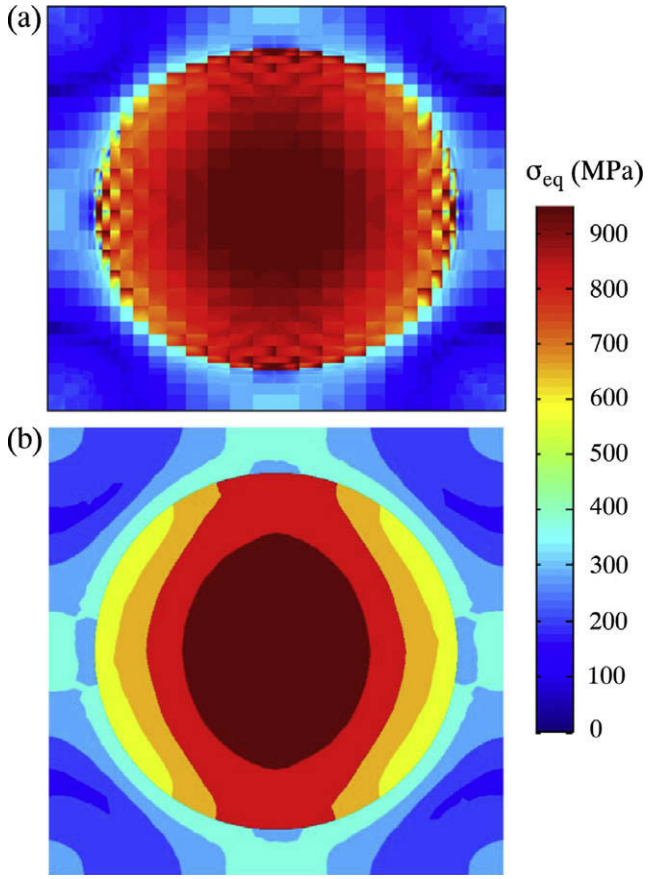

Fig. 8. Equivalent stress distribution in nonlinear glass/epoxy RUC models subject to remote transverse stress: (a) HFGMC 3D model with $(N_\beta, N_\gamma) = (32, 32)$ after convergence; (b) finite-element 2D model with generalized plane strain elements.

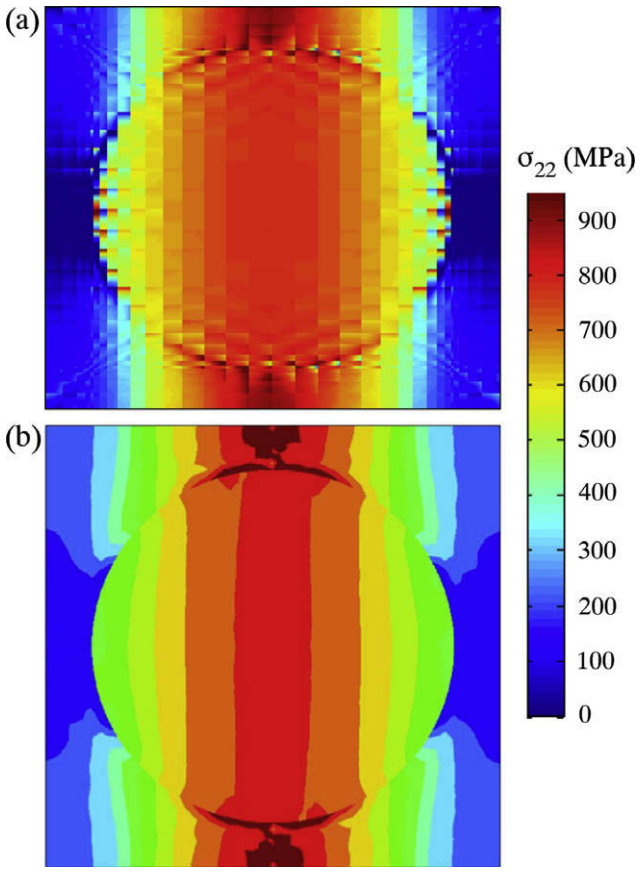

Fig. 9. Transverse stress distribution in nonlinear glass/epoxy RUC models subject to remote transverse stress: (a) HFGMC 3D model with $(N_\beta, N_\gamma) = (32, 32)$ after convergence; (b) finite-element 2D model with generalized plane strain elements.

the convergence tolerance can be either rejected (as shown in the algorithm) or kept with the anticipation of further correction to simultaneously satisfy the micromechanical relations along with the constitutive equations. The Jacobian matrix **A** of the system can be evaluated to improve the correction to the microvariable in the next iteration. It should be noted that the calculated state of the deformation fields from the previous un-converged iteration does not have to be rejected as illustrated in the iterative algorithm in Fig. 5. This is because another alternative can be followed where the current trial increment of the microvariables are kept along with the deformation state while the incremental constitutive update is performed from the previous iteration using the imposed strain correction, obtained from the differences between the strain increments of the successive iterations. As mentioned above, the algorithm in Fig. 5 is illustrated for the first case where the constitutive update is performed for a complete strain increment evaluated from the entire incremental strain after correction.

The number of solution state variables needed for the implementation of the HFGMC can vary depending on the type of nonlinear constitutive model used for each cell. The current imple-

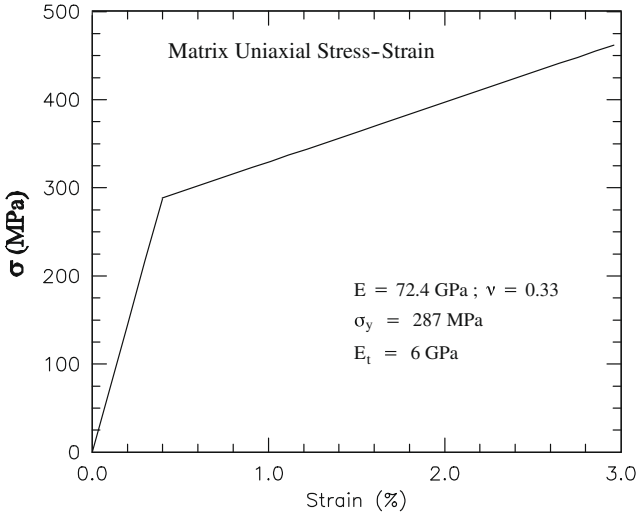

Fig. 10. Metallic matrix uniaxial elastoplastic linear-hardening stress–strain behavior.

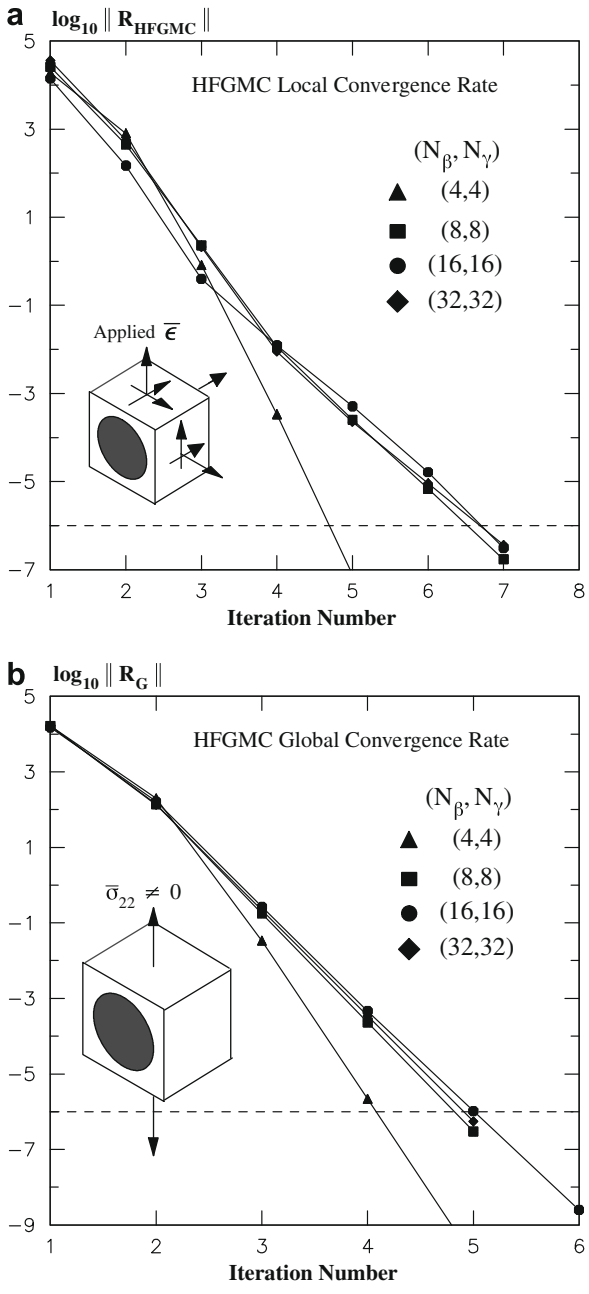

Fig. 11. Error reduction and convergence of the HFGMC for metal-matrix composite with applied transverse loading. (a) Local error convergence measure for $\mathbf{R}_{HFGMC}$ when the composite is subjected to a general multi-axial strain increment. (b) Global $\mathbf{R}_G$ convergence measure of the effort to minimize the effective stress residual.

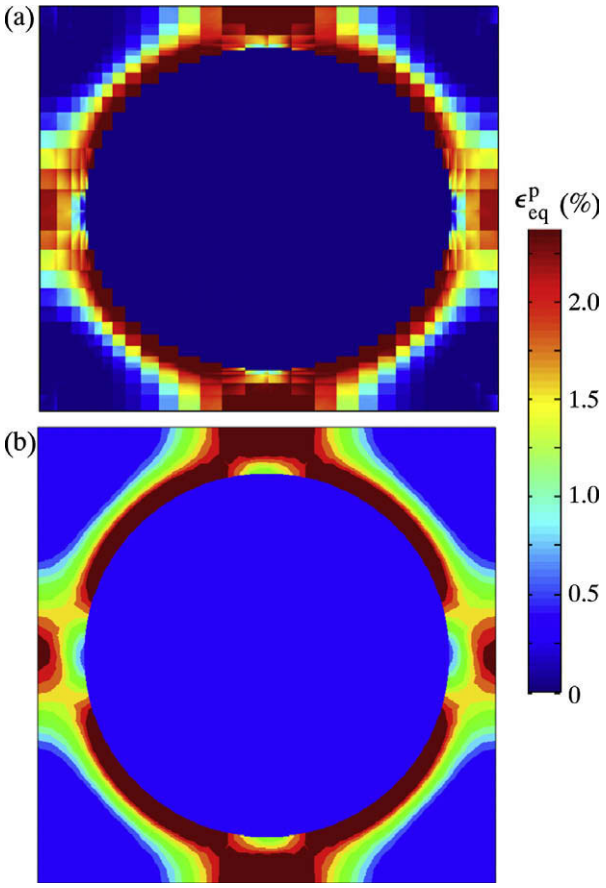

Fig. 12. Equivalent plastic strain distribution in metal–matrix RUC models subject to remote transverse stress: (a) HFGMC 3D model with $(N_\beta, N_\gamma) = (32, 32)$ after convergence; (b) finite-element 2D model with generalized plane strain elements.

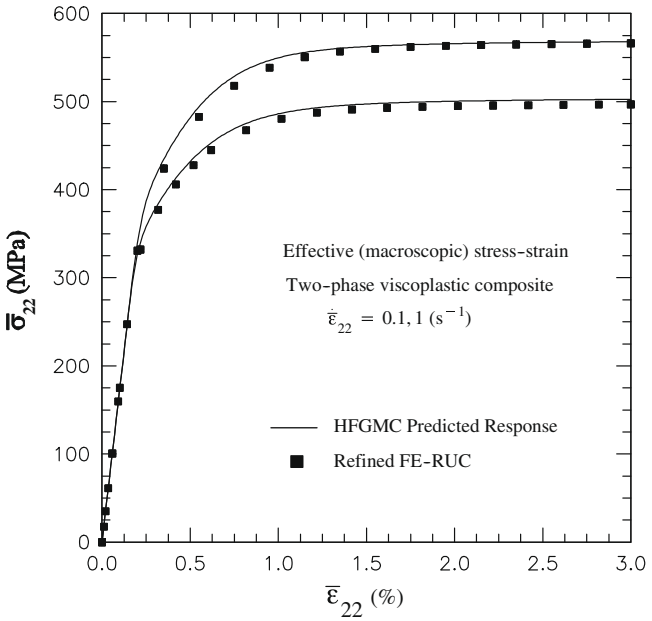

Fig. 14. Effective (macroscopic) transverse stress–strain responses of the two-phase viscoplastic composite as predicted by the HFGMC and refined FE analyses.

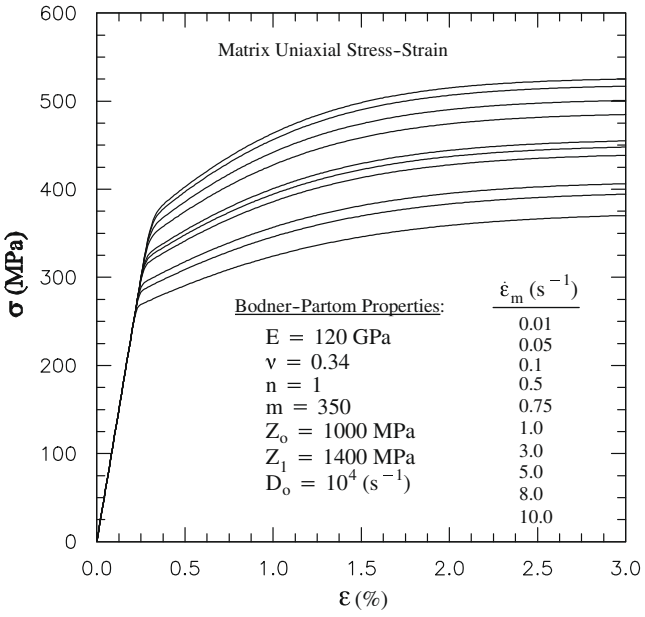

Fig. 13. Rate-dependent uniaxial stress–strain curves using the Bodner-Partom model.

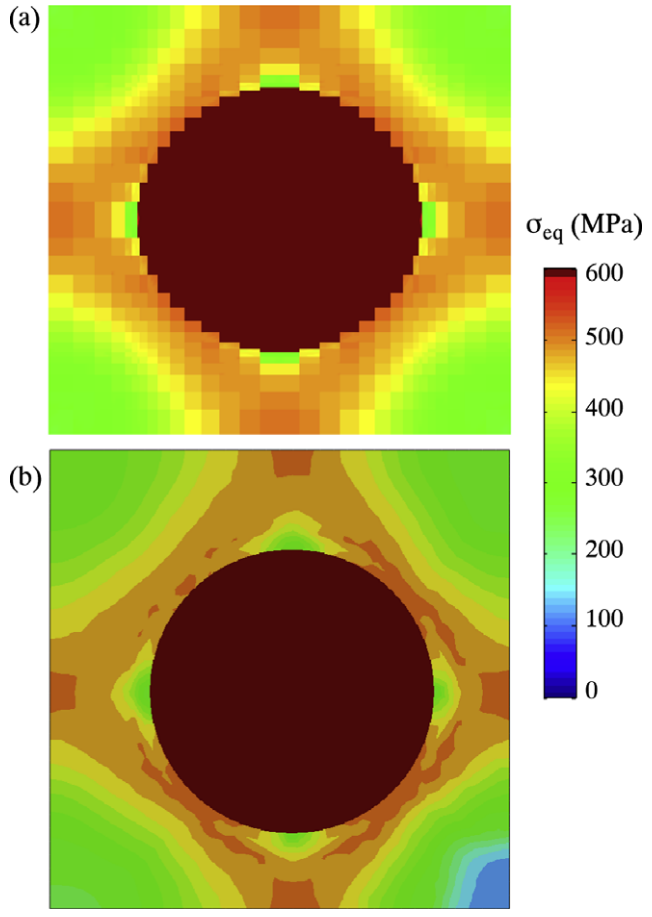

Fig. 15. Equivalent stress distribution in viscoplastic RUC models subject to remote transverse stress: (a) HFGMC 3D model with $(N_\beta, N_\gamma) = (32, 32)$; (b) finite-element 2D model with generalized plane strain elements.

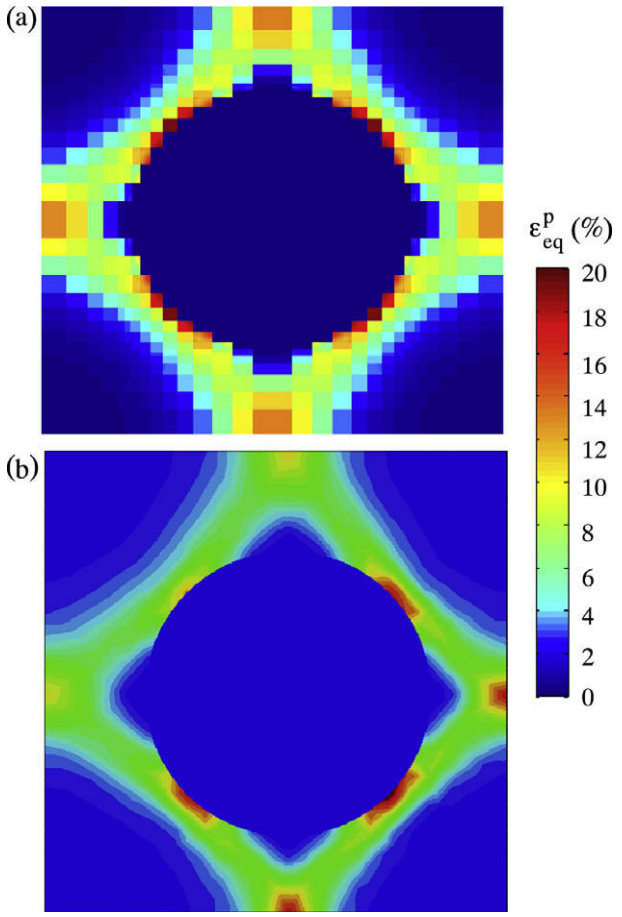

Fig. 16. Equivalent plastic strain distribution in viscoplastic RUC models subject to remote transverse stress: (a) HFGMC 3D model with $(N_\beta, N_\gamma) = (32, 32)$; (b) finite-element 2D model with generalized plane strain elements.

mentation for the constitutive relations is very similar to the strain-based incremental formulation used in a displacement-based FE environment. The number of material points used to integrate the HFGMC residual vector for each cell will multiply the number of material history variables. Therefore, the total number of material-based history variables for each cell is determined based on multiplying the number of integration points within the cell times its specific constitutive history variables. In addition there is a need to store the number of displacement microvariables for each cell. The latter is 15 for each cell that follows the doubly-periodic multiphase formulation.

It is important to emphasize that the HFGMC is not related to the classical displacement-based Finite Element (FE) method. The objective of this discussion is not to undermine the well-established FE approach rather to draw clear distinctions between these two different formulations. In the FE formulation the displacement continuity between two adjacent and connected elements is pointwise satisfied by virtue of node sharing. In the HFGMC, the displacement continuity between adjacent two cells is satisfied on an average basis. This approximation allows the HFGMC to explicitly use stress variables in the formulation and directly apply traction continuity on an average basis on common interfaces between cells. On the other hand, in the FE method nodal force equilibrium is used. Another major difference between the two methods lies in the fact that the continuum equilibrium equations are directly applied in a volumetric average at each cell, which allows retaining the cell stresses and their higher order moments in the formulation. In difference, the FE method employs equilibrium through the well known virtual work, weak flux form, expressed externally using the nodal forces. The FE is a general method and can be employed to generate micromechanical models for a priori given

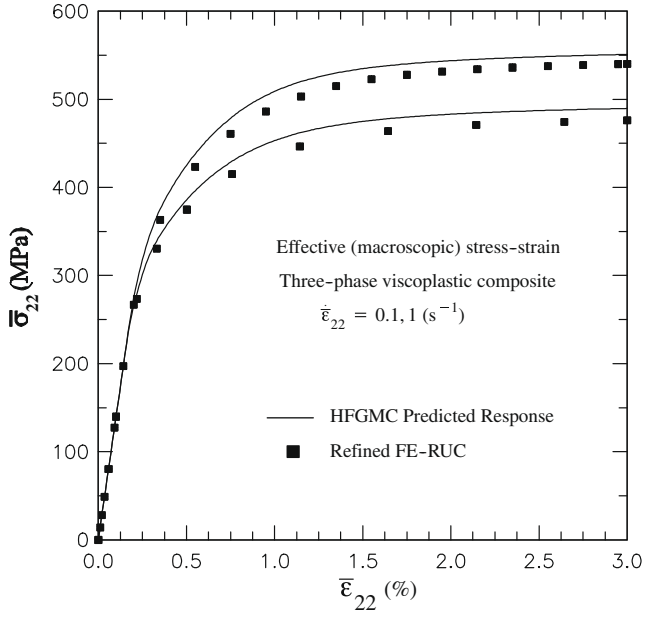

Fig. 17. Effective (macroscopic) transverse stress–strain responses of the three-phase viscoplastic composite as predicted by the HFGMC and refined FE analyses.

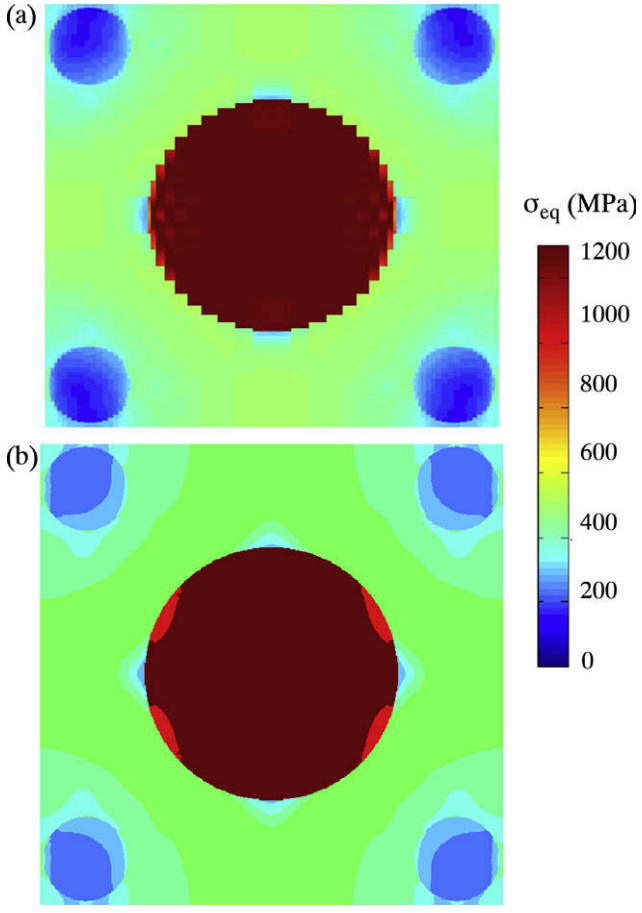

Fig. 18. Equivalent stress distribution in viscoplastic RUC three-phase models subject to remote transverse stress: (a) HFGMC 3D model with $(N_\beta, N_\gamma) = (96, 96)$; (b) finite-element 2D model with generalized plane strain elements.

states of applied remote fields. This typically requires the application of special numerical schemes needed to impose the proper remote traction and displacement boundary conditions in order to generate the correct internal fields. Unlike FE, the HFGMC is a specialized modeling framework in which the remote fields are directly tied to the micromechanical formulation (e.g., the remote average strain is directly used in the HFGMC formulation). Finally, the periodicity in the FE formulation is imposed only through displacement boundary conditions, while in the HFGMC, the periodic boundary conditions are imposed directly using both the displacement and cell tractions. Again, our aim in the above discussion is to draw clear distinctions between the two methods and not in any way claim that the HFGMC can replace the general purpose and well-established FE method.

4. Applications

Applications are performed to demonstrate the effectiveness of the proposed nonlinear micromechanical formulation. In the first application, we use the HFGMC with different number of total cells in order to predict the nonlinear transverse response of Glass/Epoxy FRP composite lamina. The fiber volume fraction v_f of this composite is taken to be $v_f = 0.5$. The fiber is considered to be linear and isotropic with a Young's modulus $E = 400$ GPa and Poisson's ratio $v = 0.2$ while the matrix is considered as nonlinear modeled by the J_2 deformation theory with the Ramberg-Osgood representation. Fig. 6 shows the nonlinear Ramberg-Osgood form of the shear stress–strain behavior along with the elastic properties for the matrix. Analyses are performed using the HFGMC with different cell array sizes N_β, N_γ to examine the convergence characteristics of the micromechanical method. A transverse load, perpendicular to the fibers, $\bar{\epsilon}_{22} \neq 0$ is applied while all other average stress components are equal to zero. This type of loading is considered a matrix-mode and typically yields pronounced nonlinear response. The analysis is set to terminate when the corresponding average strain reaches 8%. This strain level is imposed on the composite material in one increment. This is considered a rather large increment of strain as linearized solution methods usually require numerous number of increments. This verification problem, on the other hand, is aimed at testing the proposed new micromechanical solution approach and its ability to converge in this severe case. Two nested levels of iterations can be identified. The first is related the minimization of the global residual vector $\mathbf{R}_G$. For this level of convergence, the algorithm iterates to satisfy the traction free average stress, except for the imposed transverse load direction that corresponds to the applied 8% strain. The second level of iterations is directly related to the minimization of the HFGMC residual vector $\mathbf{R}_{HFGMC}$, where for each trial state of average multiaxial strain increment, the HFGMC performs its local iterative solution and convergence to the correct for the deformation fields. The convergence rate is monitored at both global and local HFGMC levels. Fig. 7(a) and 7(b) present the logarithm of the Euclidean norm of the residual error vectors, $\log_{10}\|\mathbf{R}_G\|$, $\log_{10}\|\mathbf{R}_{HFGMC}\|$, at the global and local levels, respectively, as a function of the iteration number. The convergence tolerance is set to a relatively small magnitude ($Tol = 10^{-6}$) as illustrated by the horizontal dashed lines in both figures. Since the local residual is predominately governed by interfacial tractions, one can interpret the imposed convergence criteria to be $Tol = 10^{-6}$ MPa which is very small considering that in this problem, the equivalent stress solution is of the order of 100 MPa. A more realistic tolerance will be of the order of 10^{-2} for this case. As observed, the convergence is rapid and the error can be reduced in several orders of magnitudes within few iterations. The proposed HFGMC model is able to converge for such a tight tolerance in 10 iterations or less at the most. The case of $(N_\beta, N_\gamma) = (4, 4)$ shows faster convergence rate perhaps due to the relatively smaller number of fiber cells. As the number of cells increases, the convergence trends are more consistent with each other. Having said that, no attempt is done to examine these rates from a mathematical perspective as this is considered beyond the scope of this study.

In order to examine the accuracy of HFGMC solution, a well-refined FE model is generated using generalized plane strain elements and that is subject to the same transverse loading. Fig. 8(a) and (b) show the spatial distribution of the equivalent (Mises) stress σ_{eq} in the fiber and matrix regions as predicted from the HFGMC and FE, respectively. The solution obtained from the HFGMC correlates well with the FE refined mesh solution. Similar observation can be reached from the comparison between the spatial transverse-stress distributions shown in Fig. 9(a) and (b), respectively.

The next application example is similar to the previous one, however, a metal-matrix composite is considered herein. Incremental plasticity is used for the matrix cells instead of the J_2 deformation nonlinear theory. The elastoplastic matrix uniaxial stress–strain relation is depicted in Fig. 10 where isotropic hardening behavior is assumed. The fiber is considered to be linear and isotropic with $E = 414$ GPa, $v = 0.15$ and has a volume fraction of 0.6. The matrix properties are listed in Fig. 10 where σ_y and E_t stand for the yield stress and the post yield linear hardening modulus. In this case, a 1% of transverse strain was applied in one increment. Fig. 11(a) and (b) show the norm of the error as a function

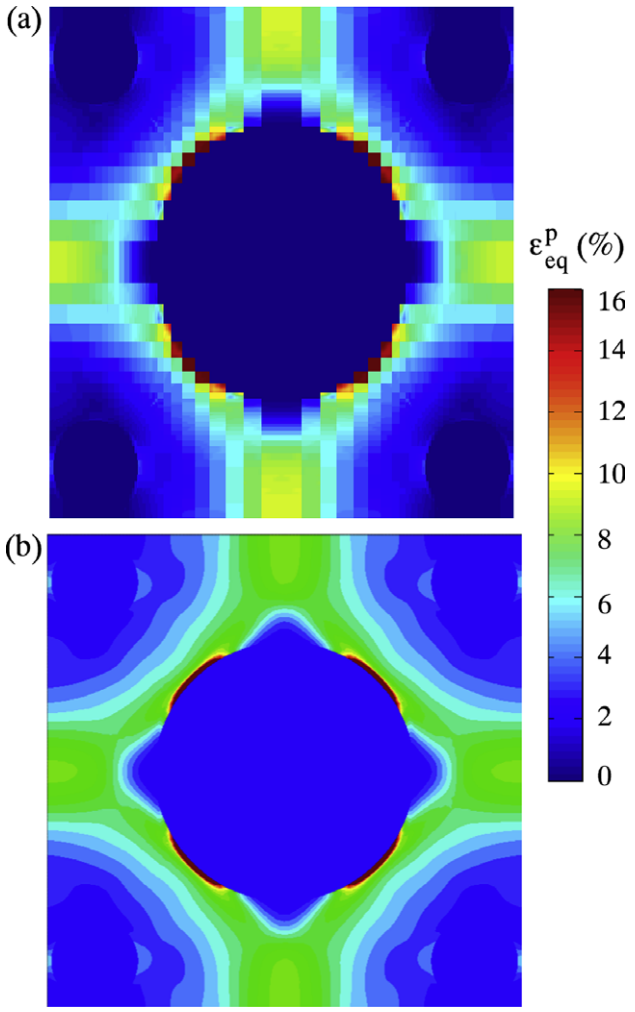

Fig. 19. Equivalent plastic strain distribution in viscoplastic RUC three-phase models subject to remote transverse stress: (a) HFGMC 3D model with $(N_\beta, N_\gamma) = (96, 96)$; (b) finite-element 2D model with generalized plane strain elements.

of iteration number for HFGMC models with different (N_β, N_γ) cell arrays. The tolerance values are indicated by the dashed lines of these figures. The convergence in this case occurs with 7 iterations or less. Similar trends of convergence are present to those in the previous polymeric matrix example. In the previous example, a comparison between the FE and HFGMC is done in terms of the spatial distribution of stresses. In the present case, Fig. 12(a) and (b) show the equivalent plastic strain ϵ^p_{eq} distributions obtained from the HFGMC and FE, respectively. Here too, good correspondence between the HFGMC and the refined FE models can be observed. It should be noted that a comparison between HFGMC and FE solutions is performed by Aboudi et al. (2003) for a metal matrix composite subjected to a transverse shear loading. In the latter case, however, the FE analysis was carried out using plane strain elements with displacements imposed on both vertical and horizontal boundaries of the RUC. Consequently, this FE model did not require global iterations. In the present investigation a drastically different comparison with FE solution is performed and reported since the net traction-free boundary conditions are achieved in all directions except in the one where the loading is imposed. In addition, only one increment of applied loading with a small number of iterations is employed using the new HFGMC formulation.

Next, let us consider the application of HFGMC to two-phase and three-phase rate-dependent (viscoplastic) composites. In the former system, the RUC consists of a circular linearly elastic fiber ($E = 414$ GPa and $\nu = 0.15$) with relatively lower fiber volume fraction of $v_f = 0.3$. The time-dependent matrix behavior is modeled using the Bodner-Partom (Bodner, 2002) unified theory of viscoplasticity. Fig. 13 illustrates the uniaxial stress–strain relations for various applied strain rates generated using the Bodner-Partom model for commercially pure titanium (highly rate-dependent). The material parameters used in the model are also listed in this figure. The predictions of the HFGMC model is compared with highly refined FE analysis using the ABAQUS software. The latter does not include the Bodner-Partom model, therefore the uniaxial stress–strain curves of Fig. 13 were used as an input to calibrate the ABAQUS FE analysis. The effective (macroscopic) transverse stress–strain responses of the two-phase composite, predicted by the HFGMC and FE models, are presented in Fig. 14 for two applied rates of transverse loading: $\dot{\bar{\epsilon}}_{22} = 1s^{-1}$ and $0.1s^{-1}$. Excellent correlation between the two methods is shown for the two rates. Figs. 15 and 16 display the spatial variations of the equivalent stress and the plastic strain distributions, respectively, within the fiber and matrix phases. Again, good correlation is demonstrated by the HFGMC when compared to the highly refined FE analysis. It should be noted that the color maps used in the contour plots are generated from two different commercial codes, namely Matlab and ABAQUS.

In order to demonstrate the versatility of the HFGMC to model multiphase viscoplastic composites, the previous RUC geometry is now modified to include a third phase in the form four additional soft fibers ($E = 12$ GPa, $\nu = 0.15$). These fibers are placed at the four corners of the RUC. The new volume fractions of the hard and soft fibers are: $v_f = 0.23$ and 0.1, respectively. Fig. 17 shows the overall response of the three-phase viscoplastic composite subject to two transverse loading rates. Figs. 18 and 19 present the local distributions of the equivalent stress and plastic strain. This combination,

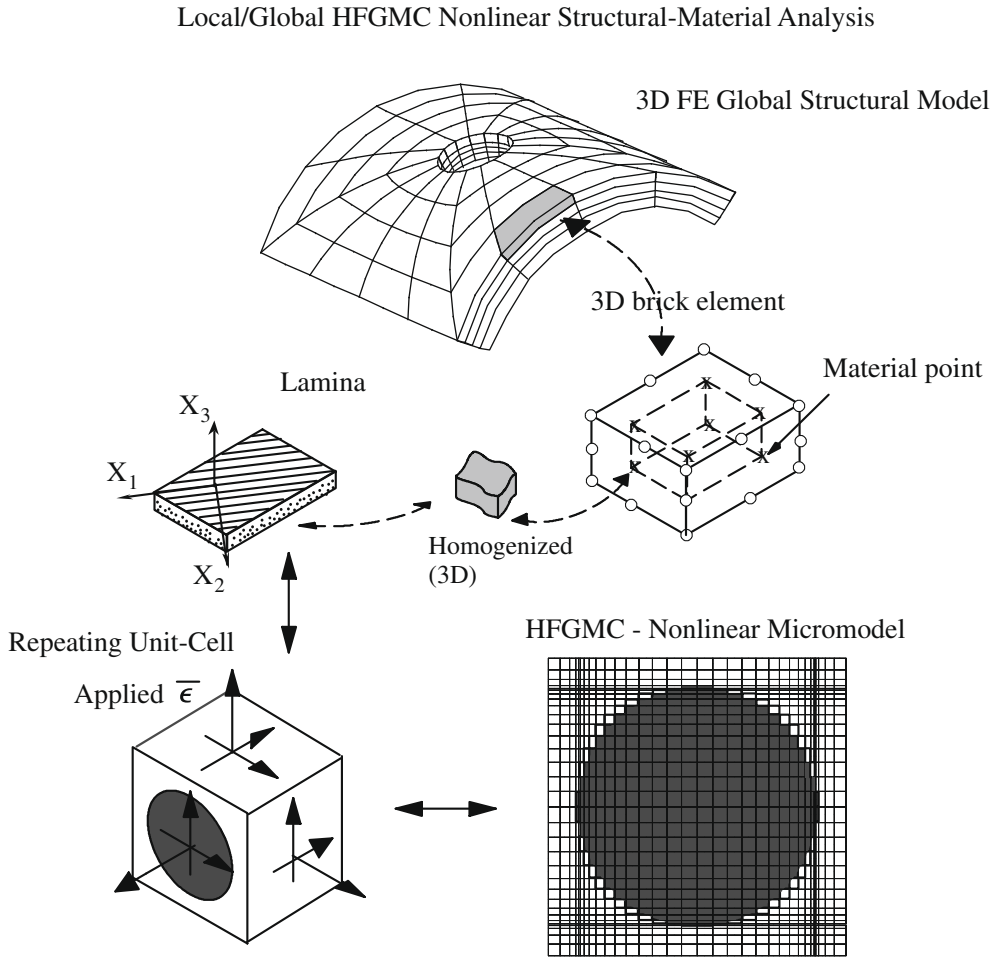

Fig. 20. Local-global material-structure framework with the HFGMC for coupled nonlinear analysis of laminated composite materials and structures.

of multiphase composite with rate-dependent constituent behavior, demonstrates the ability of the HFGMC to capture local and global responses with relatively fewer number of cells.

Thus far, the new formulation of the nonlinear HFGMC has been applied to predict the response of unidirectional polymeric and metal matrix composites. The efficiency of this new formulation enables the integration of HFGMC modeling framework to local-global structural analysis. To this end, the HFGMC was integrated with the ABAQUS (2007) general purpose implicit FE code as a material subroutine integrated to perform a coupled hierarchical analysis of composite materials and structures. Local-global analysis has been proposed for composite materials and structures with different hierarchical, concurrent and sub-structuring techniques, e.g. Fish and Belsky (1995) Fish and Shek (2000), Ghosh et al. (1995),Ghosh and Moorthy (1995) and Oden and Zohdi (1997), among several others. The new aspect of the current proposed multiscale modeling is the integration of the HFGMC nonlinear formulation and the use of its ability for selective micromechanical refinement. Fig. 20 illustrates the proposed 3D local-global nonlinear analysis where a composite structure is simulated using 3D continuum-based FE model. At each Gaussian material point in the FE element a HFGMC is implemented with different number of cells depending on the detailed microstructure level of modeling. Towards this goal, the proposed local-global modeling approach is applied to simulate the response of a notched composite thick plate shown in Fig. 21. The plate is subjected to displacement-control axial loading. The dimensions of the plate and the FE mesh are shown in Fig. 21. Two 3D brick elements are used for the two representative layers in the thickness direction. The HFGMC is applied at all Gaussian integration points in the FE elements. For most elements, the HFGMC included $(N_\beta, N_\gamma) = (4, 4)$ number of cells as shown. However, the first layer of elements around the hole (shaded area) are selected to demonstrate the ability of the HFGMC framework for increased selective modeling refinement by using $(N_\beta, N_\gamma) = (32, 32)$ for these elements. The materials properties the constituents are same as those taken in the convergence study of the polymeric matrix composite. Fig. 22 shows the structural response of the notched plate in terms of remote stress P and strain δ/L_1. The plotted symbols are the FE increments needed for the solution to reach a total of 2% remote applied strain. As it is well known that in this composite stacking, the predominant response of the laminae is in their axial shear mode $y_1 - y_2$. Fig. 23(a) and 23(b) show the distribution of the axial-shear stress σ_{12} and transverse stress σ_{22}, respectively, in the fiber and matrix

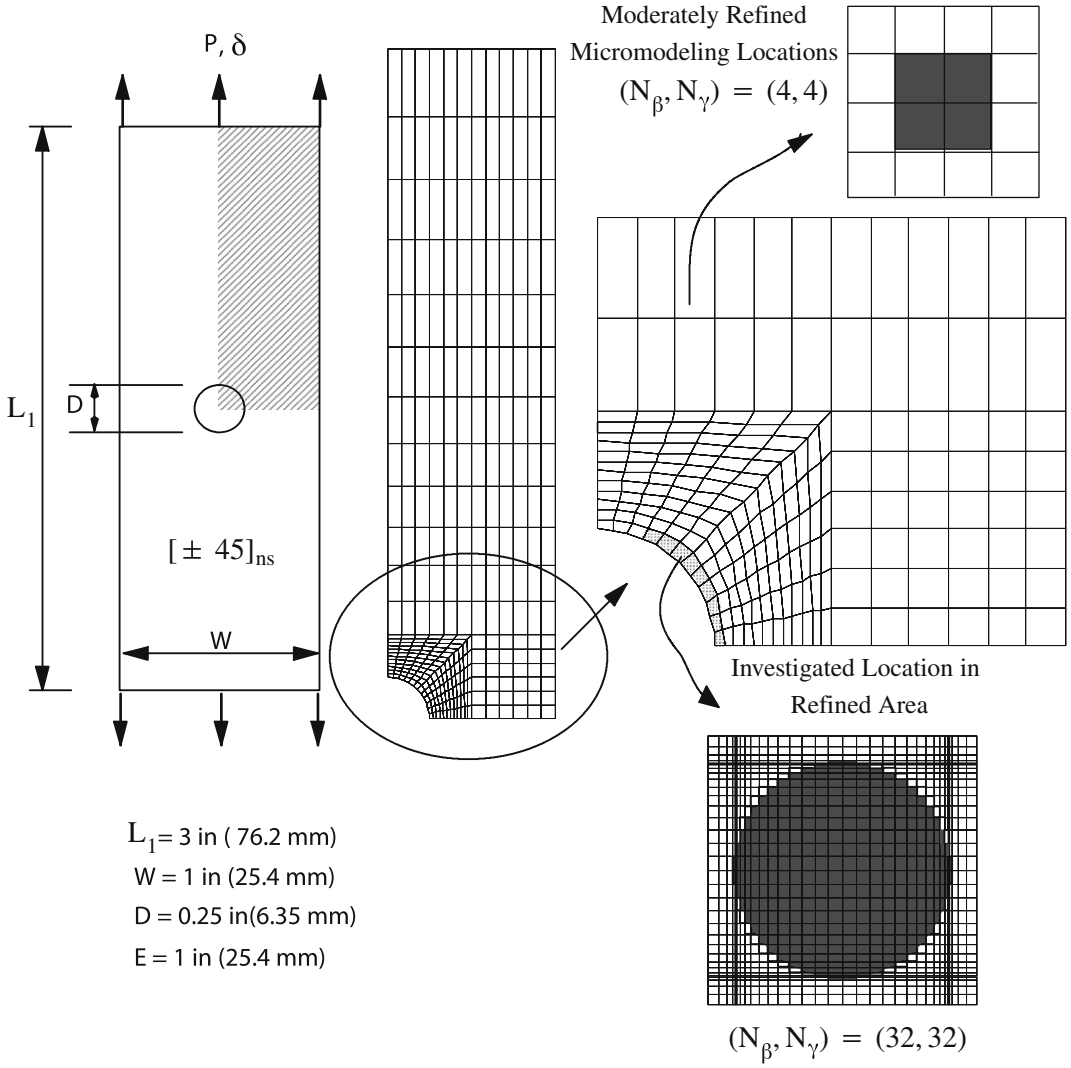

Fig. 21. Nested multiscale finite-element analysis with HFGMC model of notched laminated composite plate. The local HFGMC nonlinear micromodel is used with selective cell refinements.

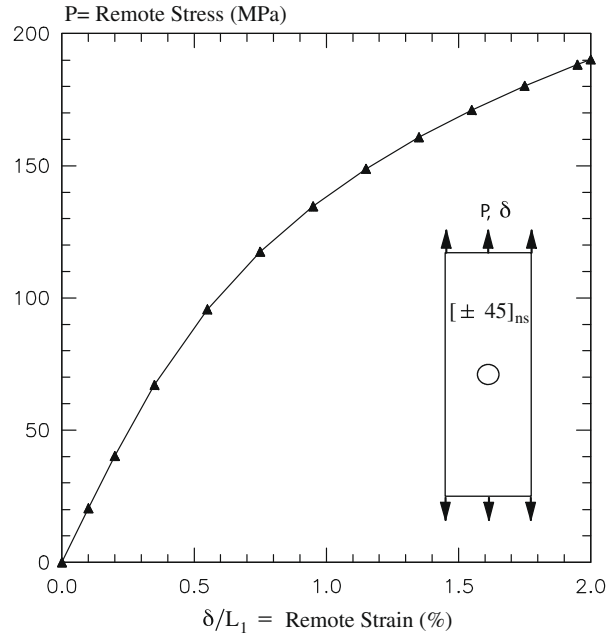

Fig. 22. Remote stress–strain of a notched composite plate.

constituents at the end of the structural simulation and for the investigated location point, in the element marked in Fig. 21. This verification analysis demonstrates a new level of refined solution capability in coupled nonlinear local-global analysis.

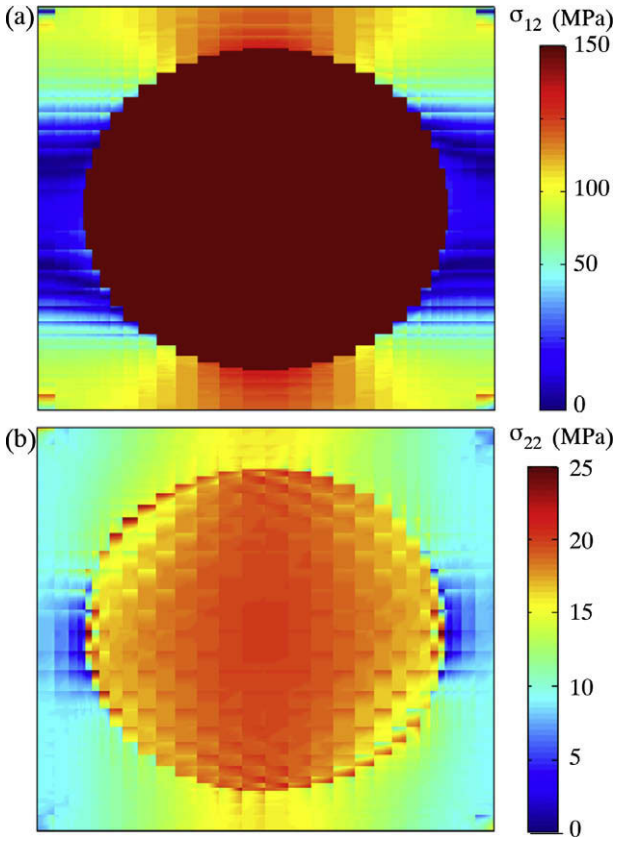

Fig. 23. Spatial distribution of shear and transverse stresses predicted from the HFGMC in a hot-spot location of the notched composite plate.

5. Conclusions

A new nonlinear micromechanical formulation of the HFGMC method is presented. This formulation facilitates an efficient numerical integration and stress correction schemes for nonlinear periodic multiphase composites under general multiaxial loading. The formulation is performed using both incremental and total stress and displacement microvariables. The incremental part allows the introduction of new compact matrix representations that can be employed to generate the effective tangent stiffness of the multiphase composite. It also enables the evaluation of the initial tangential trial deformation state in the cells. The total part of the nonlinear formulation is used to derive the residual (error) vector as well as the explicit form of its Jacobian. The latter are used in a Newton–Raphson type of an iterative scheme to correct for the trial state and satisfy both the constitutive relations in the cells along with the micromechanical equations. Applications are presented for nonlinearly elastic, elastoplastic and viscoplastic composites to demonstrate the efficiency of the proposed formulation for finite increments of imposed average stress or strain loadings. It is shown that a small number of iterations is sufficient to yield accurate solutions. Comparisons between the HFGMC models with relatively small number of cells with well-refined FE models are performed to verify the accuracy of the HFGMC models. Finally, the HFGMC formulation was implemented in a nested local-global material-structural analysis. An example is shown on how different nonlinear micromechanical modeling refinement in various locations of the structure can be achieved. The proposed formulation is general enough, and widens the application of the HFGMC for the nonlinear analysis of composite materials and structures including local effects. The generalization of the present formulation of HFGMC to triply-periodic multiphase materials is a subject for a future research.

Acknowledgement

The first author wishes to acknowledge the support of The Kahanoff Foundation and the EU Marie Curie IRG grants.

References

ABAQUS, 2007. Theory Manual, version 6.7. Dassault Systêmes Simulia Corp., Providence, RI, USA.
Aboudi, J., 1991. Mechanics of Composite Materials: A Unified Micromechanical Approach. Elsevier, Amsterdam.
Aboudi, J., Pindera, M.-J., Arnold, S.M., 1999. Higher-order theory for functionally graded materials. Compos. Part B-Eng. 30, 777–832.
Aboudi, J., 2001. Micromechanical analysis of fully coupled electro-magneto-thermo-tlastic multiphase composites. Smart Mater. Struct. 10, 867–877.
Aboudi, J., Pindera, M-J., Arnold, S.M., 2001. Linear thermoelastic higher-order theory of periodic multiphase materials. J. Appl. Mech. 68, 697–707.
Aboudi, J., Pindera, M-J., Arnold, S.M., 2003. Higher-Order theory for periodic multiphase materials with inelastic phases. Int. J. Plast. 19, 805–847.
Aboudi, J., 2004. The generalized method of cells and high-fidelity generalized method of cells micromechanical models – a review. Mech. Adv. Mater. Struct. 11, 329–366.
Aboudi, J., 2005. Micromechanically established constitutive equations for multiphase materials with viscoelastic–viscoplastic phases. Mech. Time-Dependent Mater. 9, 121–145.
Aboudi, J., 2008. Thermomechanically coupled micromechanical analysis of multiphase composites. J. Eng. Math. 61, 111–132.
Arnold, S.M., Bednarcyk, B.A., Aboudi, J., 2004. Analysis of internally cooled structures using a high order theory. Comput. Struct. 82, 659–688.
Bednarcyk, B.A., Aboudi, J., Arnold, S.M., Sullivan, R.M., 2008. Analysis of space shuttle external tank spray-on foam insulation with internal pore pressure. J. Engrg. Mat. Tech. 130, 041005–041016.
Bednarcyk, B.A., Arnold, S.M., Aboudi, J., Pindera, M-J., 2004. Local field effects in titanium matrix composites subject to fiber–matrix debonding. Int. J. Plast. 20, 1707–1737.
Bednarcyk, B.A., Yarrington, P.W., 2004. Elasto-plastic analysis of tee joints using HOT-SMAC, NASA/CR-2004-213067.
Bednarcyk, B.A., Zhang, J., Collier, C.S., Bansal, Y., Pindera, M.-J., 2006. Analysis tools for adhesively bonded composite joints. Part I: higher order theory. AIAA J. 44, 171–180.

Bodner, S.R., 2002. Unified Plasticity for Engineering Applications. Kluwer, New York.
Christensen, R.M., 1979. Mechanics of Composite Materials. John Wiley and Sons, New York.
Delannay, L., Doghri, I., Pierard, O., 2007. Prediction of tensioncompression cycles in multiphase steel using a modified incremental mean-field model. Int. J. Solids Struct. 44, 72917306.
Doghri, I., Ouaar, A., 2003. Homogenization of two-phase elasto-plastic composite materials and structures: Study of tangent operators, cyclic plasticity and numerical algorithms. Int. J. Solids Struct. 40, 16811712.
Fish, J., Belsky, V., 1995. Multigrid method for periodic heterogeneous media. Part 2: multiscale modeling and quality control in multidimensional case. Comput. Meth. Appl. Mech. Eng. 126, 17–38.
Fish, J., Shek, K., 2000. Multiscale analysis of composite materials and structures. Compos. Sci. Tech. 60, 2547–2556.
Gavazzi, A.C., Lagoudas, D.C., 1990. On the numerical evaluation of Eshelby's tensor and its application to elastoplastic fibrous composites. Comput. Mech. 7, 13–19.
Ghosh, S., Lee, K., Moorthy, S., 1995. Multiple scale analysis of heterogeneous elastic structures using homogenization theory and Voronoi cell finite element method. Int. J. Solids Struct. 32, 2762.
Ghosh, S., Moorthy, S., 1995. Elastic–plastic analysis of arbitrary heterogeneous materials with the voronoi cell finite element method. Comput. Meth. Appl. Mech. Eng. 121, 373–409.
Haj-Ali, R.M., Kilic, M., Zureick, A-H., 2001. Three-dimensional micromechanics-based constitutive framework for analysis of pultruded composite structures. ASCE J. Eng. Mech. 127, 653–660.
Haj-Ali, R.M., Kilic, M., 2003. Nonlinear constitutive models for pultruded FRP composites. Mech. Mater. 35, 791–801.
Haj-Ali, R.M., Muliana, A.H., 2004. A multi-scale constitutive formulation for the nonlinear viscoelastic analysis of laminated composite materials and structures. Int. J. Solids Struct. 41, 3461–3490.
Haj-Ali, R., 2008. Nested nonlinear multi-scale frameworks for the analysis of thick-section composite materials and structures. In: Kwon, Y.W., Allen, D.H., Talreja, R. (Eds.), Multiscale Modeling and Simulation of Composite Materials and Structures. Springer, pp. 332–371. ISBN 978-0-387-36318-938.
Haj-Ali, R.M., 2009. Cohesive micromechanics: a new approach for progressive damage modeling in laminated composites. Int. J. Damage Mech., in press.
Khan, A., Huang, S., 1995. Continuum Theory of Plasticity. Wiley, New York.
Lagoudas, D.C., Gavazzi, A.C., Nigam, H., 1991. Elastoplastic behavior of metal matrix composites based on incremental plasticity and the Mori–Tanaka averaging scheme. Comput. Mech. 8, 193–203.
Muliana, A.H., Haj-Ali, R.M., 2005. Multi-scale modeling for the long-term behavior of FRP composite structures. AIAA J. 43, 1815–1822.
Muliana, A.H., Haj-Ali, R.M., 2008. A multi-scale framework for layered composites with thermo-rheologically complex behaviors. Int. J. Solids Struct. 45, 2937–2963.
Nemat-Nasser, S., Horii, M., 1993. Overall Properties of Heterogeneous Materials. North-Holland, New-York.
Oden, J.T., Zohdi, T.I., 1997. Analysis and adaptive modeling of highly heterogeneous elastic structures. Comput. Meth. Appl. Mech. Eng. 149, 289–301.
Paley, M., Aboudi, J., 1991. Viscoplastic bifurcation buckling of plates. AIAA J. 29, 627–632.
Paley, M., Aboudi, J., 1992. Micromechanical analysis of composites by the generalized cells model. Mech. Mater. 14, 127–139.
Ryvkin, M., Aboudi, J., 2007. The effect of fiber loss in periodic composites. Int. J. Solids Struct. 44, 3497–3513.
Simo, J.C., Hughes, T.J.R., 1998. Computational Inelasticity. Springer, New York.